Water Science & Technology

Water Science & Technology Vol 87 No 6, 1393 doi: 10.2166/wst.2023.061

A comparison of struvite precipitation thermodynamics and kinetics modelling techniques

Leynard Natividad-Marin*, Max William Burns and Phil Schneider

College of Science and Engineering, James Cook University, 1 James Cook Dr, Douglas, QLD 4811, Australia
*Corresponding author. E-mail: eynard.natividadmarin@my.jcu.edu.au

LNM, 0000-0003-0184-5454

ABSTRACT

Solution thermodynamics and kinetic modelling applied to struvite crystallisation–precipitation were reviewed from diverse references to determine proximity between predicted and cited experimental measurements. These simulations show the expected variability range of struvite saturation calculation when only limited solution compositional information is given, showing acceptable agreement between predicted and experimental struvite mass. This work also compares results from struvite crystallisation kinetic studies on liquid phase species depletion, crystallisation induction time, primary nucleation, secondary nucleation, crystal growth, and crystal aggregation. Large inconsistencies between reported kinetics were observed in many scenarios. Variations in species depletion models highlighted that they are only suitably applied to the specific system from which they were regressed. Spontaneous primary nucleation was predicted to occur in the range of $SI = 0.237$–0.8. Predicted primary nucleation rates vary over at least 10 orders of magnitude (depending on supersaturation) because of uncertainties in interfacial tension and maximum achievable nucleation rate. Secondary nucleation rates are more agreeable, varying over approximately two orders of magnitude. Growth rates varied over five orders of magnitude due to variations in experimental conditions. Aggregation rates are not thoroughly examined enough to make any inferences.

Key words: aggregation, growth, kinetic, nucleation, struvite recovery, thermodynamics

HIGHLIGHTS

- Assessment of model structure and predictive capability for struvite thermodynamics in saturated systems.
- Applicability of simulations to design model validation using real effluent for struvite precipitation.
- Primary nucleation models are highly variable while secondary nucleation models are more consistent.
- Increased model complexity is required for improved struvite growth rate prediction accuracy
- Growth rate orders cannot be accurately used to infer crystal growth mechanism.

NOMENCLATURE

Symbol	Variable
β	nucleus volume shape factor
$\beta_{i,j}$	aggregation kernel between particles i and j [particles L min^{-1}]
β_0	size-independent aggregation kernel [particles L min^{-1}]
γ_s	interfacial tension/surface energy [mJ.m^{-2}]
θ	wetting angle
ν	number of ions making up a salt
τ	mean residence time of a suspension in a crystalliser working volume [s]
τ_{ind}	induction time [min]
Ω	supersaturation ratio
IAP	ion activity product
a	kinetic coefficient (size-dependent growth model) [m^{-1}]
A	induction time model constant
A'	growth rate constant (birth and spread model) [μm min^{-1}]
A''	growth rate constant (screw dislocation model) [μm min^{-1}]

A_{ind} induction time model constant
A_n nucleation pre-exponential factor/collision factor [$cm^{-3}s^{-1}$]
A_s specific crystal surface area [particles s^{-1}]
B nucleation rate used by Mehta [particles $L^{-1}s^{-}1$]
B' supersaturation constant (birth and spread model)
B'' supersaturation constant (screw dislocation/BCF model)
B_1 induction time model constant
B_2 induction time model constant
B_{ind} induction time model constant
B_{nuc} nucleation rate [particles L^{-1} min^{-1}]
C concentration [mol L^{-1}]
C_{eq} concentration at saturation/equilibrium [mol L^{-1}]
C_i concentration at the crystal interface [mol L^{-1}]
C_0 initial concentration [mol L^{-1}]
G length-based particle growth rate e [μm min^{-1}]
G_0 nuclei growth rate [m s^{-1}] (size-dependent growth model)
G_∞ large crystal growth rate [m s^{-1}] (size-dependent growth model)
J nucleation rate [particles s^{-1}]
k rate constant for species depletion model [$time^{-1}$]
k_A particle surface area shape factor
k_B Boltzmann constant $= 1.38 \times 10^{-23}$ [J K^{-1}]
k_{agg} aggregation rate constant [particles L min^{-1}]
k_d general diffusion rate constant [length $time^{-1}$]
k_g growth rate constant [μm min^{-1}]
k_r general reaction rate constant [length $time^{-1}$]
k_R species depletion model rate constant [mmol m^{-2} s^{-1}]
k_{nuc} nucleation rate constant [particles L^{-1} min^{-1}]
k_V particle volume shape factor
K_g general growth rate constant including diffusion and reaction [length $time^{-1}$]
K_{sp} solubility product
L spherical equivalent particle diameter [μm]
m crystal mass [g]
m_0 initial crystal mass [g]
n_B nucleation rate order
n_d diffusion rate constant
n_g growth rate order
n_r reaction rate order
n_R rate order in species depletion model
n_{agg} aggregation rate order
n_{nuc} nucleation rate order
n_0 nuclei population density [particles m^{-1} m^{-3}]
$n(L)$ particle population density [particles m^{-1} m^{-3}]
N particle number [particles L^{-1}]
p growth rate order in 'birth and spread' model
r_{agg} Aggregation rate [particles L^{-1} s^{-1}]
S general descriptor of supersaturation (specific measures are used in its place)
S_a (or σ) absolute supersaturation
S_r supersaturation ratio of multi-component system
SI saturation index of multi-component system
SI^* saturation index below which growth does not occur
t time [min]
T absolute temperature [K]
t_{ind} induction time [min]
v_m molecular volume [cm^3]

1. INTRODUCTION

Nutrient recovery processes are an alternative toclosing the loop of nutrients that could be eliminated in typical wastewater treatment plants. It is estimated that phosphate production costs (from rock phosphate) will increase by a factor of 3- to 5-fold in the coming century, as existing higher quality reserves are depleted (Van Vuuren *et al.* 2010). By 2100, 89% of existing

global phosphate reserves will be located in Morocco, leaving many countries dependent on importation (Cooper *et al.* 2011). Since phosphorus is a key fertiliser used in food production, efficiency in its use and reuse is of great importance for global food security. Phosphate recovery from wastewater is one element of a more sustainable food production cycle, thus this topic is being studied until recent years in real case nutrient recovery scenarios, such as urine (Volpin *et al.* 2018), livestock leachate (Martín-Hernández *et al.* 2020), and even blackwater (Sun *et al.* 2020).

Recovery by struvite crystallisation ranks higher than other technologies because of its simplicity, cost effectiveness, and safety (Mehta *et al.* 2014), and has therefore become increasingly popular. Simultaneously, there is a trend within the wastewater industry of plantwide modelling, for incorporating novel technologies (like struvite crystallisation) and for plant design and operation (Lizarralde *et al.* 2015). Therefore, precise struvite crystallisation modelling is necessary for continued improvement of wastewater treatment processes. It has been reported that the addition of magnesium to wastewater streams containing phosphorus and ammonium at alkaline conditions precipitates struvite, a mineral thatcan be used as a slow release fertiliser (Kataki *et al.* 2016; Siciliano 2016; Talboys *et al.* 2016). Consequently, suitable operating conditions for struvite precipitation have been extensively studied from empirical and thermodynamic approaches. In the first scenario, constrained experimental conditions are used to obtain an empirical model by testing different molar ratios of Mg, N, and P at different pH values (Demeestere *et al.* 2001; Capdevielle *et al.* 2013). In the second approach determination of thermodynamic equilibrium provides the advantage of assessing diverse nutrient liquid composition at diverse *pH*. Several studies had used this approach when diverse nutrient solutions were used such as synthetic urine (Liu *et al.* 2013); real urine (Ronteltap *et al.* 2007); swine lagoon (Nelson *et al.* 2003); and anaerobic supernatant (Ohlinger *et al.* 2000; Mehta & Batstone 2013).

Struvite crystallisation modelling was commonly split into thermodynamic and kinetic modelling approaches. Estimating the saturation conditions in a system can determine whether struvite precipitates at specific conditions of *pH* and nutrient composition. When solution thermodynamics is addressed, a set of '*chosen*' equilibrium equations must be solved, alongside solution chemical speciation (Ali & Schneider 2008) to determine a numerical variable representing struvite saturation, undersaturation or oversaturation. One challenge is the selection of a suitable equilibrium dataset for reliable prediction, for more simulation sophisticated approaches, such as struvite precipitation reactor design (Burns *et al.* 2021). Another challenge is selecting a suitable saturation model equation to be implemented in the kinetics approach since diverse models can be found in the literature (Buchanan *et al.* 1994; Ohlinger *et al.* 1998). Previous struvite modelling studies expressed the importance of assessing models with experimental data due to high ionic strength solution (Ronteltap *et al.* 2007), uncertainty due to model parameters such as struvite constant solubility product (K_{sp}) (Barnes & Bowers 2017), and possible presence of different solid phases (Tansel *et al.* 2018).

Solving a system of non-linear equations and thermodynamic predictions encouraged the application of specialised software packages. Within this software, we have PHREEQC (Bhuiyan *et al.* 2008; Warmadewanthi & Liu 2009; Ronteltap *et al.* 2010; Sakthivel *et al.* 2012; Ariyanto *et al.* 2014), MINTEQ (Jia *et al.* 2017), MINTEQA2 (Golubev *et al.* 2001; Nelson *et al.* 2003; Pastor *et al.* 2008; Hanhoun *et al.* 2011), MINEQL + (Kofina & Koutsoukos 2005; Bhuiyan *et al.* 2007), CHEMEQL V.2.0 (Bouropoulos & Koutsoukos 2000) and AQUASIM 2.0 (Udert *et al.* 2003a; Morales *et al.* 2013), which were run at default software configuration. This means that a diversified set of equilibrium equations and predictions could be found despite considering the same input data.

Further to constraints in the thermodynamic modelling, kinetic model limitations are examined. Kinetic models represent either a decrease of reagent concentration in the liquid phase, or the evolution of crystal mass based on the particle number and size over time. The latter approach introduces parallel mechanisms (nucleation, growth, and aggregation) which depend on each other and on system conditions. The comparison of any kinetic models is difficult as experimental and theoretical techniques and results often vary. Currently, no literature exists to provide an indication of the relative precision and accuracy of existing kinetic modelling techniques. This work compares kinetic models using a common measure of supersaturation to identify any consistent trends.

Modelling studies of thermodynamics and kinetics in struvite precipitation, however, they lacked an assessment of the mathematical equations used by different authors and a detailed comparison between them and modelling validation with cited experimental data. In this review, we compared diverse mathematical equations expressing saturation in struvite precipitation with the inclusion of additional simulations and their comparison with observed laboratory data. The review on struvite precipitation kinetics considered modelling in the liquid and solid phases, where particle nucleation, growth, and aggregation were considered. This paper indirectly highlights insightful information for other model developers working

on this topic, without introducing yet more advanced techniques such as population balance modelling (Galbraith & Schneider 2014; Elduayen-Echave *et al.* 2021), or computational fluid dynamics (Mousavi *et al.* 2019).

2. COMPARISON OF THERMODYNAMIC MODELLING TECHNIQUES

This section introduces ideas related to thermodynamic modelling in struvite precipitation, while the second part compares simulations with experimental data cited in previous research.

2.1. Solution thermodynamics modelling

2.1.1. Saturation prediction

There are different ways to express supersaturation. Supersaturation as a driving force for crystallisation/precipitation has been considered depending on only one species in solution, the difference between the concentration (C) and the equilibrium concentration (C_{eq}) described supersaturation (ΔC[1]) as shown in Equation (1):

$$\Delta C = C - C_{eq} \tag{1}$$

This method has been applied to diverse struvite investigations, considering only the limiting reagent (P or Mg) and the equilibrium concentration when this variable becomes constant (Ohlinger *et al.* 2000; Nelson *et al.* 2003; Quintana *et al.* 2005; Le Corre *et al.* 2007; Rahaman *et al.* 2008). However, this avoids chemical speciation, which is necessary for SI estimation. Avoiding chemical speciation has commonly chosen because calculations of ionic concentrations and activity coefficient to determine saturation index also implied solving a set of non-linear equations (equilibrium equations). Other works only considered a conditional solubility product (P_{cs}) in Equation (2), which evaluates when solution is likely to precipitate (Snoeyink & Jenkins 1980; Ronteltap *et al.* 2007; Ali & Schneider 2008; Rahaman *et al.* 2008). This procedure estimates the product of total elemental concentrations of Mg, N, and P ($C_{T,Mg}$, C_{T,NH_3}, C_{T,PO_4}) and compares it with a standard conditional solubility product (K_s^0) (Ronteltap *et al.* 2007). The K_s^0 is derived from the equilibrium solubility product[2] (K_{sp}) including corrections based on the ionisation fraction and activity coefficient at a specific pH, ionic strength and temperature (Snoeyink & Jenkins 1980). The supersaturation ratio (SSR) in Equation (3) was derived by representing the ratio between these two variables (Fattah *et al.* 2008; Rahaman *et al.* 2008).

$$P_{cs} = C_{T,Mg} C_{T,NH_3} C_{T,PO_4} \tag{2}$$

$$SSR = \frac{P_{s_{sample}}}{P_{s_{equilibrium}}} = \frac{P_{cs}}{K_s^0} \tag{3}$$

The ion activity product is preferrable and it is estimated with chemical speciation. Saturation level is the comparison of IAP and the equilibrium solubility product (K_{sp}). However, the mathematical equation representing the saturation index is different based on diverse authors. Additionally, the symbology of variables used in these equations also differs. Five main models based on IAP can be found:

- Supersaturation ratio is represented as (Ω) in Equation (4) (Bhuiyan *et al.* 2008).
- Absolute supersaturation: Activity-based supersaturation ratio (S_a) with the inverse of the number of ions into which a molecule dissociates ($1/\nu$) as an exponent (ν is 3 for struvite: Mg^{2+}, NH_4^+, PO_4^{3-}) in Equation (5) (Ohlinger *et al.* 1999; Mullin 2001).
- Relative supersaturation (S_r) in Equation (6), which is estimated by subtracting 1 from Equation (5) to make the saturated state zero (Bhuiyan *et al.* 2008; Mehta & Batstone 2013).
- Reduced supersaturation in Equation (6).
- Saturation Index (SI) in Equation (7), which is derived from Equation (4), with the inclusion of the logarithmic expression.

[1] The concentration difference ΔC is sometimes interchanged with the variable S (Mullin 2001)

[2] K_{sp} can take different values from 12.60 (Stumm & Morgan, 1996) to 13.26 (Ohlinger et al., 1999). In this work the last value will be considered for later simulations.

- An alternative saturation index, termed SI* here for clarity in Equation (8), which is derived from Equation (5), also with the inclusion of a logarithmic expression (Ali & Schneider 2008; Triger *et al.* 2012).

Another alternative description, only listed here due to its specific use in a struvite investigation (Hanhoun *et al.* 2013), defines saturation as the difference between IAP and K_{sp}, including the inverse power of the number of ions in Equation (9). This has been termed as S_h here for distinction between other saturation definitions.

For the purpose of comparing crystallisation rates, a number of supersaturation descriptors are necessary. Variables are given in the nomenclature and detailed descriptions can be found in any number of struvite texts (Ohlinger *et al.* 1998; Ronteltap *et al.* 2007; Bhuiyan *et al.* 2009; Galbraith & Schneider 2014).

$$\Omega = \frac{IAP}{K_{sp}} \tag{4}$$

$$S_a = \sigma = \Omega^{1/\nu} = \left(\frac{IAP}{K_{sp}}\right)^{1/\nu} \tag{5}$$

$$S_r = S_a - 1 = \Omega^{1/\upsilon} - 1 \tag{6}$$

$$SI = \log_{10}(\Omega) = \log_{10}\left(\frac{IAP}{K_{sp}}\right) \tag{7}$$

$$SI^* = \log_{10}(S_a) = \log_{10}\left[\left(\frac{IAP}{K_{sp}}\right)^{1/3}\right] = \frac{1}{3}\log_{10}\left(\frac{IAP}{K_{sp}}\right) \tag{8}$$

$$S_h = IAP^{1/3} - K_{sp}^{1/3} \tag{9}$$

The saturation index (SI) in Equation (7) has been widely applied in struvite precipitation research (Wang *et al.* 2006; Iqbal *et al.* 2008; Warmadewanthi & Liu 2009; Tilley *et al.* 2009; Ariyanto *et al.* 2014; Galbraith & Schneider 2014). Logarithm scale in this expression provides the advantage of overcoming many numerical issues where species concentrations can vary over many orders of magnitude between each other. The IAP represents the interactions of all ions driving precipitation. The logarithm of IAP and K_{sp} becomes zero when saturation is reached, and this value can be incorporated into crystal growth rate functions.

Equation (10) also introduces saturation as the potential for struvite recovery ($P_{struvite}$). This equation is a function of ion molar activities and K_{sp} to correlate the quantity of possible struvite (Tao *et al.* 2016). In this expression, HPO_4^{2-} was used instead of PO_4^{3-}, and it was supposed to better represent the nutrient recovery potential instead of SI at pH 8.5–9.5 (Tao *et al.* 2016).

$$P_{struvite} = \frac{(Minimum\{Mg^{2+}\}\{NH_4^+\}\{HPO_4^{2-}\})^3}{K_{sp}} \tag{10}$$

However, this affirmation is incorrect because the maximum quantity of struvite that is possible to obtain depends on the ionic chemical species from the limiting reagent quantity (Mg or P in most cases). Moreover, it is logical that prediction of SI should include the ionic components in struvite. Thus, whatever the value of predicted SI, the quantity of struvite can only be estimated when elemental mass balance and chemical speciation are considered.

2.1.2. Activity coefficients and ionic strength

The calculation of activity coefficients depends on valences (Z_i) and ionic strength (μ). Debye–Hückel limiting law in Equation (11) is commonly used when μ is less than 5×10^{-3} M, and Guntelberg modification in Equation (12) when $\mu < 0.1$ M (Sohnel & Garside 1992). Debye–Hückel modified by Davies model in Equation (13) (cited as 'Davies' from now on) has been extensively used to estimate mean activity coefficients (Harada *et al.* 2006; Ali & Schneider 2008; Schneider *et al.* 2013; Galbraith *et al.* 2014), where 'a' is 1 and 'b' can be −0.2 or −0.3 at 25 °C depending on the years (1938 or 1962) (Sohnel & Garside 1992). The maximum μ recommended for the use of this equation varies according to authors, with some considering an appropriate μ as up to 0.2 M (Mullin 2001), while another suggested 0.5 M (Ronteltap *et al.* 2007). Therefore,

application to dilute wastewater treatment streams is usually accepted, while the application in high concentration nutrient source should be carefully considered. For instance, the addition of magnesium to nutrient solutions could cause deviations in the activity coefficient estimation since the resulting μ after mixing can be 0.5 M or higher. In this scenario, Bromley Equation for μ up to 6 M (Sohnel & Garside 1992) has been suggested (Ali 2007); however, the ionic contribution parameters required in the model, such as HCO_3^-, $MgHCO_3^+$, $MgPO_4^-$, $NaHPO_4^-$, $MgOH^+$, $CaPO_4^-$ and $CaOH^+$ are not specified, and excess of ammonium compounds made it inappropriate (Bromley 1974) and less suitable unless more parameters are found.

$$-\log_{10}\gamma = 0.5Z_i^2\mu^{1/2} \tag{11}$$

$$-\log_{10}\gamma = 0.5Z_i^2\left[\frac{\mu^{1/2}}{1+\mu^{1/2}}\right] \tag{12}$$

$$-\log_{10}\gamma = AZ_i^2\left[\frac{\mu^{1/2}}{1+a\cdot\mu^{1/2}} + b\cdot\mu\right] \tag{13}$$

An alternative to this dilemma is the application of a modified version of the Davies equation cited in Equation (14), referred to here as Samson's equation. This model has been used for solutions with ionic strength up to 1.2 M (Samson *et al.* 1999). This expression depends on μ, Z_i and other parameters such as A′ (1.172), B′ (3.33×10^9), and a′ (3.0×10^{-10}). It was applied in crystallisation studies but not specifically in struvite precipitation (Barsanti *et al.* 2009; Fevotte *et al.* 2013). One of the most likely situations where ionic strength could surpass 0.50 M is in the nutrient recovery of undiluted urine nutrient source since previous studies have shown an ionic strength between 0.32 and 0.56 M using synthetic and real solutions (Ronteltap *et al.* 2007).

$$\ln\gamma = -A'Z_i^2\left[\frac{\mu^{1/2}}{1+a'\cdot B'\cdot\mu^{1/2}}\right] + [-4.17\times10^{-15}\cdot\mu + 0.2]\cdot A'\cdot Z_i^2\cdot\frac{\mu}{1,000^{1/2}} \tag{14}$$

Figure 1 shows the importance of selecting the correct model in the estimation of activity coefficients, depending on the ionic strength magnitude. This plot shows the two versions of 'Davies' (1938 and 1962) and 'Samson' models at different ionic strengths, which highlights a most coherent prediction of Samson's model especially at higher ionic strength. All the models achieved close predictions up to $\mu = 0.10$ M; from 0.10 to 0.30 M, deviations become visible, especially in the case of 'Samson' model, showing a decreasing tendency. At $\mu > 0.3$ M, 'Samson' model continues decreasing, while the two

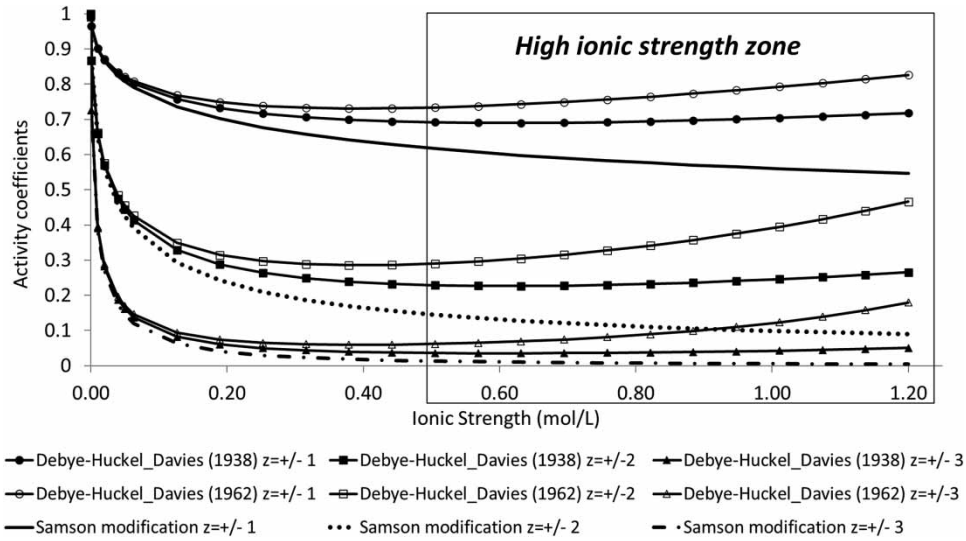

Figure 1 | Activity coefficients' prediction with different models as a function of ionic strength. *Note*: This plot has been elaborated by the authors of this paper with EES software using Equations (13) and (14).

versions of 'Davies' showed an atypical increasing trend of the activity coefficients, indicating that the Samson model is more appropriate for modelling higher concentration solutions. Comparison between 'Davies' model version shows that the 1962 model has a higher increment than its older 1938 version. The application of 'Samson' model as an alternative was also compared with a more sophisticated model such as Pitzer, with similar prediction up to 1.4 M ionic strength solutions (Fevotte *et al.* 2013). Selection of the suitable model will depend on the ionic strength of the nutrient; however, it remains unclear whether choosing a 'Davies' model in the range close to 0.5 M provides logical predictions in struvite precipitation studies.

2.1.3. Predicting saturation in real effluents

Struvite precipitation simulations can determine the struvite saturation index (*SI*) at non-equilibrium conditions, or the maximum possible struvite mass after desaturation after a very long time (close to equilibrium conditions). These two scenarios are calculated by resolving the model for one of two states: (1) prediction of *SI* when struvite mass is set as zero, and (2) prediction of the maximum quantity of formed struvite when *SI* is set to zero (or close to zero). A numerical solver capable of solving non-linear equations, such as Engineering Equation Solver (EES) (F-Chart Software, Madison, WI, USA) has been previously used to include a set of equilibrium equations, activity coefficient model (Davies model), chemical speciation, charge balance and liquid–solid mass balance to study the batch precipitation of struvite (Ali & Schneider 2008; Galbraith 2011). Thermodynamic equilibria and solubility constants of solid phases (Babić-Ivancić *et al.*, 2006; Gadekar & Pullammanappallil, 2009; Musvoto, 2000; Nordstrom *et al.*, 1990; Ohlinger *et al.*, 1998; Udert *et al.* 2003b; United States EPA, 1998; Xu *et al.*, 2015) cited in Supplementary material, Tables A1 and A2 are also included. Even though this approach is useful to predict struvite precipitation in synthetic solution, its application in real effluents is even more challenging due to a more complex liquid composition, because this type of composition could require a larger set of equilibrium relationships.

Simulations of struvite precipitation in real effluents require some considerations in the initial input given to the programme. One way to solve the system is by introducing the *pH* of the system as an input variable and allowing the charge balance to be calculated instead of being set as zero (Gadekar & Pullammanappallil 2009). Therefore, this approximation introduces the inquiry if a struvite precipitation system with too little compositional information can be successfully predicted with a small deviation from real measurements. In this scenario, simulations could be used to estimate an output variable (e.g. pH, struvite quantity, total dissolved P concentration) range when a different quantity of elements is considered or when set *pH* is changed assuming an error in the measurement. The influence of selected thermodynamic equations could be also assessed since they are related to the quantity of elements considered in the system. As species concentration measurement can be time consuming, evaluating the possibility of decreasing the quantity of input simulation data warrants consideration while maintaining an acceptable level of accuracy.

2.2. Solution thermodynamic simulations

2.2.1. Thermodynamic software applications

In this work, simulations were run in PHREEQC Interactive 3.7.3 software to determine the struvite saturation index in saturated solutions. This software offers several chemical speciation models (equilibrium constant databases). Each of these calculations in several synthetic and real struvite precipitation scenarios were tested to determine variability in saturation index predictions (especially struvite). PHREEQC is a thermodynamic simulation software that has been used in previous studies, but few had reported the used database (Roncal-Herrero & Oelkers 2011; Sakthivel *et al.* 2012), arising the possibility of answer diversification despite the same input data. To corroborate the previous comment, six struvite precipitation laboratory experiments previously cited were simulated (Table 1). In these simulations, total elemental concentration, *pH*, and temperature were set as input data; and 7 of the 13 available databases in the software[3] were tested. The struvite formation chemical reaction and the constant solubility product of 13.26 (Ohlinger *et al.* 1998) were introduced in each simulation. In the following, each experimental case is discussed targeting key information and the calculated saturation index.

- The first case (Nelson *et al.* 2003), where nutrient solution was exposed to $pH = 8.4$, 8.7 and 9.0, shows that only 'minteq.v4' and 'sit' databases predicted results accordingly to observations of solid formation. Databases: 'minteq.v4' and 'sit' databases predict positive saturation index of other solids containing *Mg* and *P* with diverse quantities of water molecules. This situation could suggest that experimental identification of the solid phase is needed. For instance, previous works

[3] The reader should be aware that previous PHREEQC versions (~ 2016) only had 9 available databases, and this quantity could keep changing in the future.

Table 1 | Saturation index prediction of solid phases in nutrient recovery scenarios, using different databases provided by PHREEQC software package

Struvite precipitation cases and considered input data for simulations		Prediction of Saturation Index using diverse databases within PHREEQC							References
		minteq.v4	wateq4f	phreeqC	sit	minteq	llnl	iso	
1) Swine wastewater: 23 °C, units (mol/L): Mg (1.92×10^{-3}), N (1.01×10^{-2}), P (1.63×10^{-3})	a) pH = 8.4	0.77, $(0.01)^2$	−27.97	−27.97	1.04, $(1.94)^1$	0.68	−28.1	−27.97	(Nelson *et al.* 2003)
	b) pH = 8.7	−1, $(0.61)^2$	−28.95	−28.95	1.27, $(2.55)^1$, $(0.38)^2$, $(0.45)^3$	−1.16	−29.08	−28.95	
	c) pH = 9.0	−3.09, $(1.21)^2$	−29.97	−29.97	−0.22, $(3.13)^1$, $(0.96)^2$, $(1.03)^3$	−3.37	−30.11	−29.97	
2) a) Synthetic digested liquor: 25 °C, pH (8.4), units (mol/L): Mg (2.62×10^{-3}), N (4.50×10^{-2}), P (1.74×10^{-3}), Cl (4.64×10^{-2})		0.84	−27.82	− 27.82	1.56 $(1.77)^1$	0.79	−27.87	−27.83	(Quintana *et al.* 2005)
b) Real digested liquour: 25 °C, pH (8.81), units (mol/L): Mg (2.62×10^{-3}), N (4.50×10^{-2}), P (1.74×10^{-3}), Ca (1.22×10^{-3}), C (2.11×10^{-2})		−2.02 (*)	−29.24 (*)	−29.24 (*)	1 (*)	−2.18 (*)	−29.29 (*)	−29.24 (*)	
3) Synthetic nutrient solution: 25 °C, pH (9.0), units (mol/L): Mg (3.5×10^{-3}), N (7×10^{-3}), P (7×10^{-3}), Cl (7×10^{-3})		−3.38, $(2.4)^2$, $(0.25)^4$	−29.75	−29.75	−0.70, $(4.21)^1$, $(2.29)^2$, $(2.10)^3$, $(0.18)^4$	−3.78	−29.81	−29.75	(Le Corre *et al.* 2007)
4) Raw wastewater adjusted with chemical reagents: 37 °C, pH (8.5), units (mol/L): Mg (1.00×10^{-1}), N (1.00×10^{-1}), P (1.00×10^{-1}), Ca (5.29×10^{-4}), K (5.50×10^{-2})		−1.30, $(5.61)^2$, $(1.83)^4$ (*)	−26.86 (*)	−26.86 (*)	1.36, $(7.09)^1$, $(6.64)^2$, $(4.96)^3$, $(1.61)^4$ (*)	−1.56 (*)	−26.45 (*)	−26.86 (*)	(Türker & Celen, 2007)
5) Synthetic supernatant: 20 °C, pH (8.51), units (mol/L): Mg (1.28×10^{-3}), N (4.28×10^{-2}), P (9.85×10^{-4})		1.12	−28.06	−28.06	1.35 $(1.18)^1$	1.07	−28.31	−28.06	(Rahaman *et al.* 2008)
6) Synthetic nutrient: 25 °C, pH 8.0, units (mol/L): Mg (8.27×10^{-3}), N (4.78×10^{-2}), P (6.52×10^{-3})		2.09, $(1.23)^2$, $(0.44)^4$	−25.74	−25.74	2.07, $(3.08)^1$, $(1.16)^2$, $(0.97)^3$, $(0.38)^4$	2.04	−25.80	−25.75	(M. Iqbal *et al.* 2008)

Notes: Struvite *SI* are the unparenthesis values; and parenthesis values with superscripts indicate: (1) Bobierite $Mg_3(PO_4)_2.8H_2O$, (2) Magnesium Phosphate $Mg_3(PO_4)_2$, (3) Cattite $Mg_3(PO_4)_2.22H_2O$, (4) Newberyite $MgHPO_4.3H_2O$. Additionally: (*) Positive saturation index in solid phases containing Calcium.

have experimentally shown the presence of newberyite and possible bobbierite when the molar ratio Mg:N:P are 1.5:1:1 using X-ray diffraction (Burns *et al.* 2016). Moreover, experimental data were collected from 2-L samples of anaerobic swine lagoon liquid, and elemental analysis was performed with Inductively Coupled Plasma spectrometry (Nelson *et al.* 2003).

- The second case (Quintana *et al.* 2005) simulated two sub-cases for struvite precipitation: synthetic liquor and real digested liquor. In the simulations, the total elemental carbon concentration was assumed to be equivalent to the molar concentration of $CaCO_3$ (akalinity). Similarly to the first case in the paragraph above, 'wateq4f', 'phreeqC', 'llnl' and 'iso' databases provide a very negative struvite saturation index, and a positive saturation index for $N_2(g)$ which can be explained by the selected database, such as the presence of N_2 as a species in 'phreeqC' database and its absence in 'minteq' database, which leads to different chemical speciation of nitrogen. By not considering the presence of molecular $N_2(g)$, the chemical speciation of total nitrogen to their ionic species can predict higher NH_4^+, and therefore struvite presence making the 'phreeqC' and 'minteq' the suitable ones for this case. Moreover, experimental data were collected from 1 L beaker solutions, using plasma emission spectrometry to measure elemental concentration in the liquid phase (Quintana *et al.* 2005).
- The third case (Le Corre *et al.* 2007) predicted *SI* from a synthetic solution in the higher *Mg* concentration added to the reactor (3.5 mM in $MgCl_2.6H_2O$) and a Mg:N:P equivalent to 1:2:2. The temperature was set as 25 °C since it was not mentioned in this research, while the *pH* was 9.0 after adjustment with *NaOH*. This research also claimed struvite identification with scanning electron microscopy although no results were shown. Simulations predicted a negative saturation index for struvite with a wide result range, in which four databases predicted a very negative struvite saturation index (~ -30) similar as the previous two cases, two databases (minteq.v4, minteq) in the range of -3, and one database with a value close to zero (sit). It is obvious that the latter provides the prediction of more solid phases within the database. These results suggest that addition of *Mg* in a lower molar ratio compared to *P* could not trigger precipitation of struvite, but other similar solid phases such as magnesium phosphates with different quantities of water molecules. However, it is not possible to suggest the absence of struvite unless solid phase characterisation is developed. Moreover, experimental data were developed in 600 mL volumetric flask.
- The forth case (Türker & Celen 2007) predicted *SI* during precipitation with anaerobic digester effluent as a nutrient source. This study provided an approximate wastewater composition, citing ionic concentrations of NH_4^+, Mg^{2+}, and PO_4^{3-} in mg/L. This research considered that previous data were being expressed as the main elemental concentration (e.g. NH_4^+-N 'ammonium expressed as nitrogen', PO_4^{3-}-P 'phosphate expressed as phosphorus') as it is commonly described in analytical methodologies (APHA 1999). A temperature of 37 °C was entered in PHREEQC, since laboratory experiments were developed at typical anaerobic digester effluent temperature. Working at a different temperature than 25 °C required the adjustment of struvite solubility product to 13.269 (at 37 °C) (Babić-Ivančić *et al.* 2002) in the entry data. No variation in the final concentration of Ca^{2+} and K^+ after adding H_3PO_4 was considered since the volumetric information was not given. All the previous notes also highlight the importance of clear and explicit information for modelling research. Moreover, the experimental study was developed using 200 mL effluent with standard elemental analysis (APHA 1999).
- The fifth case (Rahaman *et al.* 2008) predicted *SI* in struvite precipitation with a synthetic solution. This study comprised nine experiments with a focus on struvite production kinetic in 2-L jars, and only the first case was simulated with PHREEQC. This experiment was accomplished by adding *Mg* to the nutrient solution (Mg/P molar ratio $= 1.3$). Due to compositional simplicity of this case, not many positive saturation indexes of other solids were computed. Positive struvite *SI* was observed in 'minteq.v4', 'sit' and 'minteq' databases, adding the possibility of bobierite in the latter. Moreover, the analysis of ortho-phosphate and ammonia was obtained with the flow injection method (LaChatChem 8000 instrument), while magnesium concentration was measured with atomic absorption spectrophotometry (Varian Inc. SpectrAA220 Fast Sequential Atomic Absorption Spectrophotometer) (Rahaman *et al.* 2008).
- The sixth case (Bhuiyan *et al.* 2008) discussed the solid formation with anaerobic digester effluent. This research explores kinetics of struvite precipitation, including the metastable zone for struvite and struvite saturation index prediction with PHREEQC. Simulation developed in this work only used the second metastable experiment at $pH = 8.0$, when $PO_4 - P$, $NH_4 - N$, and Mg were set as 202, 669, and 201 mg/L, respectively. The second condition was selected because the Mg/P molar ratio was closer and above the unit (1.3), while the others had excessive *Mg* addition or a Mg/P molar ratio lower than one. The original source reported an estimated struvite $SI = 2.14$, which is very close to the one found in this

work when 'minteq.v4' (2.09), 'sit' (2.07), and 'minteq' (2.04) databases were explored. Deviation between this work and the original source can be explained by the assumed struvite constant solubility product (13.36) in the original source. With this entry data, other positive saturation indexes can be found, especially with 'sit' database. Moreover, laboratory measurements were obtained with the flow injection method for elements different than magnesium, and fame atomic absorption spectrophotometry for magnesium (Bhuiyan *et al.* 2008).

Based on previous estimations, it is clear that 'sit' database estimates higher *SI* for struvite and predicts the presence of other solid phases. This outcome makes this database the most reliable among the others for quick solution thermodynamic predictions. The high variability of *SI* estimations also means that equilibrium database selection should be informed when PHREEQC (or similar software) is applied. It is recommended that a suitable database is selected by assessing all possible options to find the one that represents experimental observations and measurements. It is also recommended that thebest fit to purpose model would be constructed manually. These results highlight the importance of understanding model architecture, which is the subject of the subsequent sections.

2.2.2. Data entry and model predictions

One key enquiry when modelling struvite precipitation from the real rich-nutrient waste stream is the quantity of compositional data needed to achieve close to reality predictions. Predictions could be further from experimental measurements if insufficient elemental composition is given to the simulator. To explore this idea the case 2.b in Table 1 (Quintana *et al.* 2005) was simulated infour scenarios by this authors' paper, considering the different quantities of chemical elements and combinations: (1) *Mg*, *N*, *P*, *C*, *Ca*; (2) *Mg*, *N*, *P*, *C*; (3) *Mg*, *N*, *P*, *C*a; and (4) *Mg*, *N*, *P*.

In this paper, the authors solved equilibrium equations, mass balance, charge balance and chemical speciation in a set of the linear and non-linear equations, considering previous modelling and simulation approaches (Harada *et al.* 2006; Ali & Schneider 2008; Schneider *et al.* 2013; Galbraith *et al.* 2014). Simulation results are shown in Figure 2, which was split based on key variables for further model implementation in Figure 2(a) (non-equilibrium), and model validation (equilibrium) in Figure 2(b) and C[4]. In addition, struvite was considered as the only solid phase present to facilitate the estimation of struvite mass at equilibrium. These simulations were performed with the model developed in EES described in section 2.1.3 and PHREEQC using 'sit' database.

In Figure 2, experimental data from previous work (Quintana *et al.* 2005) was compared with simulations developed by the authors of this paper.

Figure 2(a) shows an increasing struvite *SI* trend ($\sim$ 0.10 to 0.20) when fewer elements are considered. This can be explained by the presence of higher concentrations of Mg^{2+}, NH_4^+, and PO_4^{3-} when other ions are not present and therefore cannot capture part of the ions to precipitate other solid phases (e.g. $Ca_3(PO4)_2$). This plot also presents larger differences between each applied model suggesting that the set of equilibrium equations provide more variability compared to the compositional data. Even though the inclusion of additional elements in the estimation can slightly change the *SI*, this variation can be significant if it is included in other more complex modelling studies (such as kinetics). It is an important reminder that struvite *SI* cannot be measured directly, and therefore other measurable variables must be assessed in similar studies.

Predictions and measurements of total phosphorus concentration and the struvite mass are shown in Figure 2(b) and 2(c), respectively. While it is logical that variations are expected, the observed variations are notably large. Figure 2(b) shows a predicted dissolved *P* concentration in PHREEQC almost ten times the concentration predicted in EES. This result is logical if it is compared with the predicted struvite *SI* in Figure 2(a), recalling that *SI* is a logarithmic variable (Equation (7)). The molar concentration of the measured dissolved *P* in the liquid phase after precipitation was taken from the cited work (5.07 mg/L), and it is within the prediction range. A larger measured *P* concentration compared to the prediction by EES means an overprediction of the struvite *SI* in Figure 2(a). Previous logic could be applied in the PHREEQC predictions, showing again the importance of collecting reliable experimental concentration measurements in the liquid phase to adjust models.

[4] This work considers the term 'equilibrium condition' to the one in which a variable achieves a constant value. In the original source: 240 min for *P* concentration to get a minimum after struvite precipitation started.

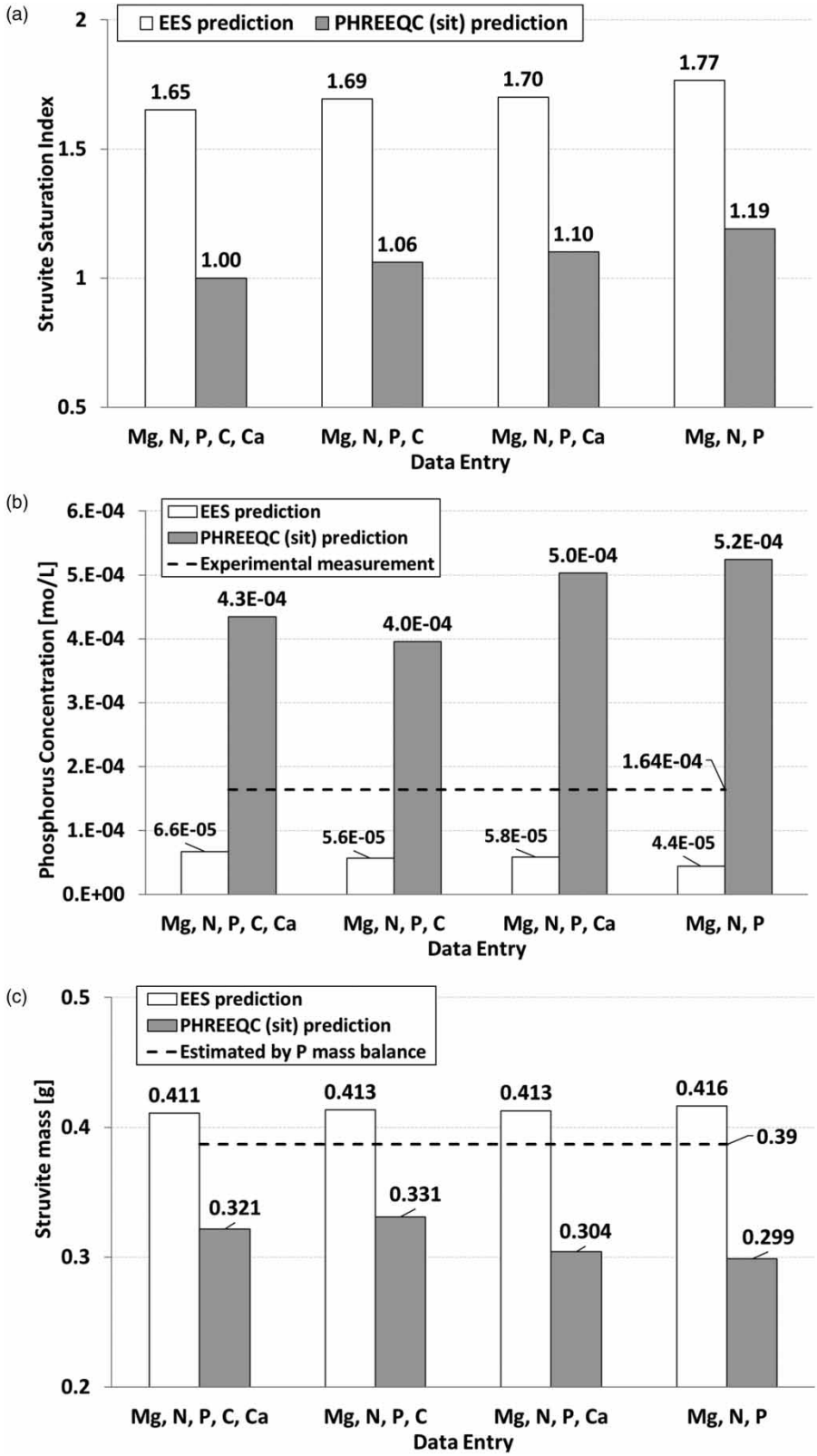

Figure 2 | Struvite precipitation from real digested liquour (case 2.b in Table 1) by discussing struvite *SI* at non-equilibrium (a), dissolved P (b), and struvite (c) at equilibrium conditions.

The experimental struvite mass in Figure 2(c) was estimated by subtracting the initial P concentration in the nutrient (before precipitation) and the remaining P concentration after desaturation (in the liquid phase at equilibrium). It was also assumed 1 L of nutrient solution with negligible volume change after precipitation. In the EES simulation, the volume was introduced to estimate the struvite mass, while PHREEQC considers a default value of 1 kg when no value is introduced. Figure 2(c) is clearly related to the other two plots by suggesting an over precipitation of struvite with EES and an under precipitation with PHREEQC. However, percental deviations in struvite mass (predicted vs. measured) are small in Figure 2(c) if we compare them to the P dissolved concentration in Figure 2(b). Therefore, assessing model validation in struvite precipitation becomes a more rigorous task if the liquid concentration is chosen over struvite mass in the validation since the range of P in the liquid is much smaller than P in the solid phase.

2.2.3. Model validation in a batch reactor

The model developed by this research group in EES (Harada *et al.* 2006; Ali & Schneider 2008; Schneider *et al.* 2013; Galbraith *et al.* 2014), which was previously explained in this paper, was tested against published data of struvite precipitated from real urine source in a set of 21 batch experiments (Ronteltap *et al.* 2007). The original work (Ronteltap *et al.* 2007) applied PHREEQC combined AQUASIM software packages to estimate struvite solubility product and equilibrium molar concentration of P and Mg. The EES programme, which was previous cited, was applied by introducing the measured total concentrations of Mg, N and P, $pH = 9$, and setting equilibrium (i.e. $SI = 0$) held after leaving the solution to reach a minimum concentration in the liquid phase. These simulations were performed with both Debye–Hückel modified by Davies and Samson's version models to observe differences at high ionic strength (close to 0.50 M).

Figures 3 and 4 compared measurements (Ronteltap *et al.* 2007) and predictions from the original source (Ronteltap *et al.* 2007) and this paper's predictions, providing strong similarities, and showing that the thermodynamic model used in this work was suitable to describe nutrient recovery from urine source, and 'Davies' model still provides logical predictions. This information also suggested that the main solid phase in the precipitated product was struvite because simulations were developed with this assumption and agreement was found. Predicted and experimental data of elemental P and Mg concentrations at different Mg/P feed molar ratios in Figures 3 and 4 can also suggest which of them should be measured in model validation. For instance, choosing lower Mg/P (<1) can be suitable for P measurements, while much larger Mg/P could relate P concentration lower than the detection limit. The same logic applies to model validation when Mg should be selected at $Mg/P > 1$. The selection of the chemical element to measure during model validation depends on the compositional data, which is related to the instrumental detection limit.

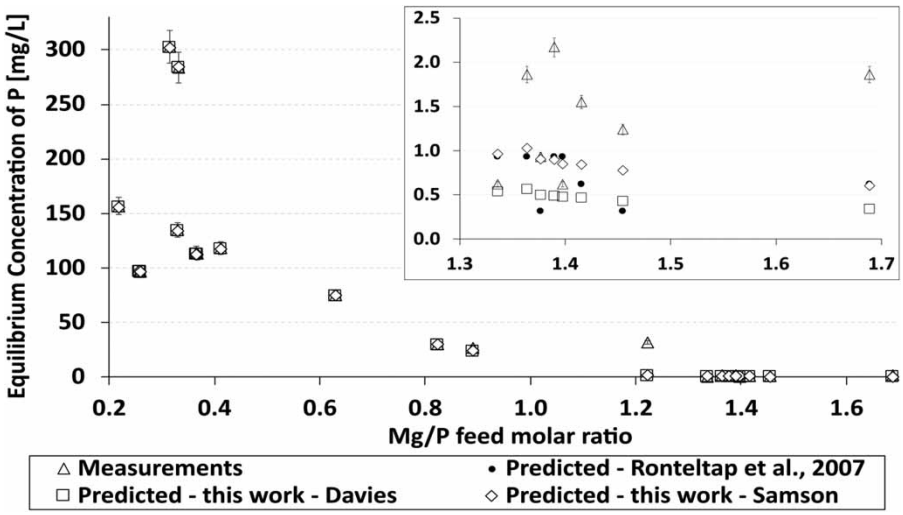

Figure 3 | Model validation at equilibrium using P concentrations. Error bars are ±1 standard deviation.

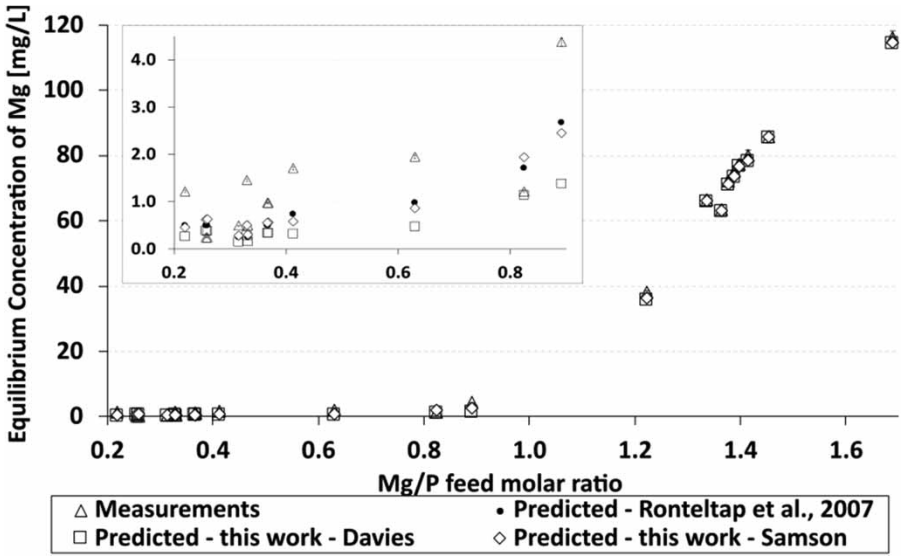

Figure 4 | Model validation at equilibrium using Mg concentrations. Error bars are ±1 standard deviation.

3. COMPARISON OF KINETIC MODELLING TECHNIQUES

Once a description of the driving force for crystal formation has been developed, the rate of crystal formation can be examined.

3.1. Induction time

The beginning of crystallisation is described by a reducing time interval between reaching a given super-saturation ($SI > 0$) and achieving measurable crystal formation. This time interval is known as the induction time (τ_{ind}). Induction time models are based on the classic primary homogeneous nucleation theory that induction time is inversely proportional to nucleation rate, which is only valid at high saturation levels (Mullin 2001) and while nucleation is approximately steady state (Jones 2002). The molecular process of nuclei formation remains contested (Laxson & Finke 2014), making a true definition of induction time difficult. Ions must coagulate, resist the tendency to re-dissolve, and become oriented into a fixed crystalline lattice (Mullin 2001).

Most struvite induction time studies (Table 2) assume that nucleation time is much greater than growth time, causing induction time to be defined as the time needed to form a critical nucleus. This time cannot be measured, and the induction time becomes the time taken for a particle to grow to a detectable size. Table 2 shows that differences in particle detection methods influence induction time estimations.

While two forms of the induction time model have been applied to struvite, they differ only in their representation of super-saturation, but are equivalent. Bouropoulos & Koutsoukos (Bouropoulos & Koutsoukos 2000) and Bhuiyan (Bhuiyan & Mavinic 2008; Iqbal *et al.* 2008) both used the first form of this equation (A and B_1) given by Mullin (Mullin 2001), which uses Ω, given by Equation (4), as the measure of saturation.

$$\log \tau_{ind} = \log A + \frac{B_1}{(\log \Omega)^2} = \log A + \frac{B_2}{(\log S_a)^2} \tag{15}$$

where A is constant and B_1 is givens by:

$$B_1 = \frac{\beta \upsilon_m^2 \gamma_s^2}{(2.303 k_B T)^3} \tag{16}$$

where β is a nucleus volume shape factor (32 for cubes and $16\pi/3$ for spheres), υ_m is the molecular volume of struvite (=molecular weight/(Avogadro's number × density × number of ions in a formula unit) = 7.95×10^{-23} cm^3 for struvite), γ_s is the interfacial tension (i.e. surface energy) of the solid which is forming, k_B is the Boltzmann constant

Table 2 | Reported induction time model conditions and homogeneous nucleation saturation level

Author	pH range (max pH reached)	Experimental saturation range (*SI*)	Phosphate conc. [mM]	Molar ratio *Mg:N:P*	Reactor type	Mixing speed [rpm]	Method of nucleation detection	Induction time range [min]	Lowest saturation for homogeneous nucleation (*SI*)
Bouropoulos & Koutsoukos (2000)	8.5	0.05–0.52	2.75–4.00	1:1:1	250-mL double-walled vessel	N/A	*pH* change (0.005)	6–125	0.30
Bhuiyan & Mavinic (2008)	8.2–8.51	1.38–1.83	1.81–3.39	1:22.1:1.3	2-L square beaker	120	*pH* change	0.2–8.33	N/A
Mehta & Batstone (2013)	N/A	~0.42 to ~0.85	100	1:1:1	200-mL glass bottles	300	*pH* change (0.05)	0.167–60.79	0.69
Ohlinger *et al.* (1999)	6.3–7.9	0.61–1.47	4–20	1:1:1	Pyrex beaker, no specified capacity	570	Light scintillations	0.22–38	N/A
Galbraith & Schneider (2009)	7.8–9.2	0.04–0.31	1.0–2.5	1:1:1	250-mL beaker	Quiescent	Light scintillations	16.65–438.15	0.237
Le Corre *et al.* (2007)	9	0.88–1.52	2.4–4.6	1:2:2	250-mL beaker and 10-L FBR	Quiescent/ unknown	*pH* change	~0.5–5 (beakers) 6–12 (reactor)	N/A
Kabdasli *et al.* (2006)	8.438–9.228	0.371–1.135	2.45	1:1:1	1,500-mL cylindrical glass reactor	300	Absorbance	~1–46	N/A
Saidou *et al.* (2009)	8.2	Calculated	3.8	1:1:1	1-L aerated FBR	N/A	P and Mg concentration	5–17	N/A
Kofina & Koutsoukos (2005)	8.5	0.318–0.633	2.2–3.0	1:1:1	250-mL double-walled Pyrex vessel thermostated	Teflon-cotated stirring bar (no speed specified)	*pH* change (0.005)	~0 to ~67	0.502–0.643

(1.38×10^{-23} [$J\ K^{-1}$]) and T is the absolute temperature. Others used the second induction time equation form (A and B_2) which uses S_a, described by Equation (5), as the measure of saturation (Ohlinger *et al.* 1999; Galbraith & Schneider 2009; Mehta & Batstone 2013). Again A is constant, while B_2 is identical to B_1 except in this instance includes the number of ions into which a molecule of the crystal dissociates, ν, which accounts for the different measures of saturation:

$$B_2 = \frac{\beta v_m^2 \gamma_S^3 f(\theta)}{(2.3 k_B T)^3 \nu^2} \tag{17}$$

where $f(\theta)$ is a correction factor to account for heterogeneous nucleation, where θ is the wetting angle of the solid phase by the liquid. $f(\theta) = 1$ for homogeneous nucleation. This model has been applied successfully to heterogeneous nucleation (Randolph & Larson 1988; Ohlinger *et al.* 1999).

Although homogeneous nucleation is asserted during measurements of induction time, heterogeneous primary nucleation (induced by suspended particles) is much more likely, both in lab environments and in real solutions. This is especially true at low supersaturation levels. Many authors have identified a supersaturation level where homogeneous nucleation ceases to occur (summarised in Table 2). The transition between homogeneous and heterogeneous nucleation is commonly defined as the intersection of two linear regressions made on a $(\log(\Omega))^{-2}$ vs. $\log(t_{ind})$ plot. However, applying the homogeneous induction time model at low saturations has been identified as a questionable technique (Mullin 2001).

Many investigations have been made into struvite induction time, the results of which vary depending on experimental methods and analysis techniques. Table 2 provides a consolidation of struvite induction time investigations, showing that the lower saturation bound for struvite homogeneous nucleation has been predicted to occur anywhere in the range of $SI = 0.237 - 0.69$. Figure 5 provides a comparison of model predictions of induction times over a range of SI values. As nucleation is defined by the identification of crystallisation, it is dependent on the method of crystal detection. Light scintillation detected nucleation at the lowest saturation (SI = 0.237) although a change in pH also detected nucleation at a similar saturation index (SI = 0.3). Higher saturation level, mixing speed, and the ratio of P to other constituents generally results in a lower identified induction time.

Figure 5 shows that induction time increases exponentially below $SI = 0.8$, irrespective of the model parameters adopted. However, it has also been shown that scaling can occur in the continuous flow where induction time models predicted that it should not (Burns *et al.* 2016). This was attributed to larger residence times in the slow moving viscous sub-layer. Variations in induction time parameters within the literature have been attributed to many effects, including variations in detection methods, mixing speeds and reagent ion ratios (Galbraith & Schneider 2009). In any instance, it must be assumed that induction time models carry significant uncertainty.

When induction time is reached and crystal formation begins, the formation rate can be represented with various mathematical descriptions, each with its benefits and trade-offs. Generally, the struvite mass formation rate is calculated using

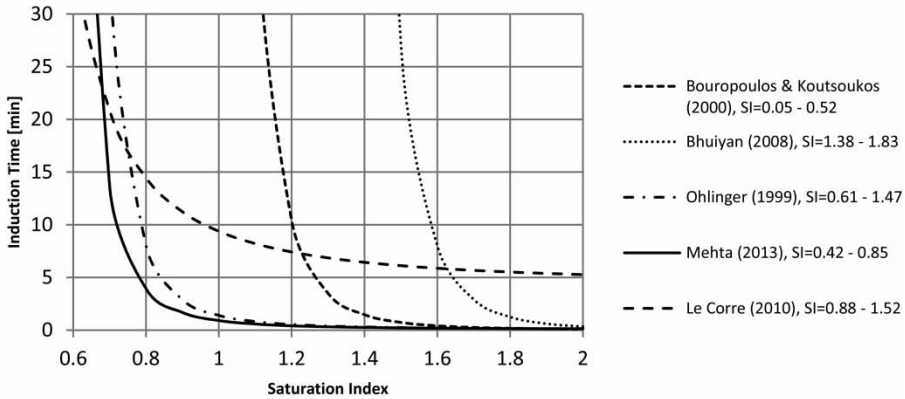

Figure 5 | Induction time model comparison was created using methods described by Galbraith & Schneider (2009) and incorporating more recent data (Le Corre *et al.* 2007; Mehta & Batstone 2013). Results from Mehta & Batstone (2013) were calculated using induction time model parameters rather than thermodynamic modelling, as raw data were not provided. The model from Bhuiyan, Mavinic & Beckie (2008) was not considered accurate as pH change was used to identify the end of induction time in a solution which likely had significant ammonia buffering (N:P ratio of 17:1).

two different kinetic models: rates of liquid phase species depletion and rates of individual crystal formation mechanisms. These categories are discussed in more detail in the following sections.

3.2. Liquid phase species depletion rate

Most commonly, struvite kinetics have been modelled using a first order power law model (Equation (18)) where the limiting reagent concentration is used to describe the driving force for crystallisation. Stoichiometry is then used to infer concentration depletion and crystal mass.

$$\frac{dC}{dt} = kS^n \tag{18}$$

where C is the concentration of the species in question, t is some measure of time, S is some measure of supersaturation and k and n are the rate constant and order. A first order kinetic model ($n = 1$) has been extensively applied, which when integrated, using individual species concentration as the supersaturation measure, gives Equation (19), where C, C_{eq} and C_0 are the concentrations of the reactant at time t, at equilibrium and at time 0 respectively (Ohlinger *et al.* 2000; Nelson *et al.* 2003; Quintana *et al.* 2005; Le Corre *et al.* 2007; Rahaman *et al.* 2008; Ariyanto *et al.* 2014).[5]

$$\ln(C - C_{eq}) = -kt + \ln(C - C_0) \tag{19}$$

Several experimental factors have been shown to influence the regressed rate constant. Primarily pH and Mg:P ratio, both of which are factors that affect struvite ionic species concentration. Increasing Mg:P ratio significantly increased rate constants under a variety of conditions (Quintana *et al.* 2005; Rahaman *et al.* 2008). Additionally, increasing the starting pH from 8.4 to 9.0 increased the rate 3x with the same caustic dosing rate (Nelson *et al.* 2003). Other factors including temperature, ionic strength, and mixing speed have a smaller but still noticeable effect on regressed rate constants (Rahaman *et al.* 2008; Ariyanto *et al.* 2014).

Each of these studies suggests that a more detailed kinetic model is necessary to represent the struvite system over a range of conditions. The correlation of rate with ion ratio suggests that the use of a single species in a reaction equation is flawed. Struvite kinetics are likely better described using a measure of saturation incorporating the ion activity product so that all struvite constituent concentrations contribute to the rate description. Other physical properties of a system like a temperature may also warrant consideration in kinetic model formulations if they are likely to change significantly.

Substituting $n = 2$ into Equation (18) and integrating gives Equation (20), a second order model. Some struvite research, in which faster growth rates have been observed, has found that a second order kinetic model provides a reasonable fit (Bouropoulos & Koutsoukos 2000; Türker & Celen 2007; Bhuiyan *et al.* 2008).[6] While this approach fits each dataset, the methods and results of each of these studies are not comparable.

$$\frac{1}{C} = \frac{1}{C_0} + kt \tag{20}$$

A more detailed approach to species depletion was used by Mehta, who applied a power law model to describe struvite molar deposition rate, using reduced supersaturation ratio (S_r) as the driving force (Equation (21)). Change in crystal surface area was accounted for using the initial and final mass of the crystal, assuming size-independent growth (*SIG*) and no nucleation (Mehta & Batstone 2013).

$$\frac{dC_{MAP}}{dt} = k_R A_s \left(\frac{m}{m_0}\right)^{\frac{2}{3}} S_r^{n_R} \tag{21}$$

[5] Quintana used MgO to determine kinetics, although this was not the limiting reagent according to molar ratios Mg:P>1 in plots, making their results questionable.

[6] Bhuiyan converted the diffusion-reaction model from a mass deposition to a particle linear growth rate with the knowledge of total particle mass, average particle diameter and solution volume.

where C_{MAP} is the struvite concentration [mM], k_R is the rate constant (0.09 ± 0.04 mM·m^{-2}.s^{-1}), A_s is the specific surface area of the seed crystals before growth occurs [m^2/L], m_0 and m represent the crystal mass initially and at any time and n_R is the growth rate order. The struvite particle growth rate exhibited a higher dependence on SI in real wastewater than in synthetic wastewater, highlighting that results are not transferrable between the two systems. The growth order was regressed to be 3.52 ± 0.1, significantly higher than first and second order models discussed above.

Each species depletion model may be accurate within the conditions under which they were derived, but this is not useful for application to varying conditions. The alternative approach to using a liquid phase species depletion rate is to model individual crystallisation mechanisms. Crystal growth can be broken down into nucleation, growth and agglomeration. In all of the above examples, these mechanisms have been neglected or merged. The following sections introduce mechanisms of crystallisation and identify deficiencies in the struvite crystallisation literature.

3.3. Nucleation

3.3.1. Primary nucleation

The thermodynamic approach to representing primary nucleation utilises the Arrhenius reaction velocity equation used to represent thermally activated processes. The derivation, which can be found in Mullin (Mullin 2001), assumes spherical nuclei and uses the Gibbs–Thompson relationship between particle size and solubility. The Gibbs–Thompson relationship only applies for particles $<1\,\mu$m but not for extremely small particles, meaning that nuclei are assumed to lie in this bracket. The resulting expression of nucleation rate (J [s^{-1}]) is given by:

$$J = A_n \exp\left(-\frac{16\pi\gamma^3 v^2}{3k_B^3 T^3 (\ln\Omega)^2}\right) \tag{22}$$

where A_n is a kinetic factor (/pre-exponential factor/collision factor) with units [$cm^{-3}s^{-1}$], k_B is the Boltzmann constant ($1.38 \times 10^{-23} J/K$), Ω is the saturation ratio, γ is the interfacial tension between the crystal and the solution [mJ/m^2] , v is the molecular volume [cm^3] (described by Equation (16)), and T is the absolute temperature. If this expression is generalised to include the particle volume shape factor ($k_V = V/L^3$) and surface area shape factor ($k_A = SA/L^2$) it can be written as:

$$J = A \exp\left(-\frac{192 k_V^2 \gamma^3 v^2}{k_A k_B^3 T^3 (\ln\Omega)^2}\right) \tag{23}$$

The kinetic factor A has been assumed to be 10^{17} nuclei·cm^{3-} for struvite (Abbona & Boistelle 1985; Bouropoulos & Koutsoukos 2000) although according to the Gibbs–Volmer theory, sparingly soluble salts should have a kinetic factor in the range of $\approx 10^{25}$ nuclei·cm^{-3}. In contrast to these high rates, one study found the value of A to be between $10^{4.47}$ and $10^{6.6}$ nuclei·cm^{-3} by manually varying it to achieve the best fit between experimental and modelled supersaturation (Hanhoun *et al.* 2013). Computation of A based on nucleation studies is possible but would still rely on an assumed value for interfacial tension, which would itself relies on previous kinetic factor estimates.

The interfacial tension γ has been found to be 15, 48, and 50 mJ/m^2 (Abbona & Boistelle 1985; Bouropoulos & Koutsoukos 2000; Kofina & Koutsoukos 2005; Bhuiyan *et al.* 2008). The variation of Kofina's result ($15\ mJ/m^2$) was attributed to interference by excess SO_4^{2-} ions, which is logical as γ is inversely proportional to a salt's solubility (Mullin 2001). Results from induction time experiments conducted by Ohlinger assumed that struvite interfacial tension would be similar to that of silica ($78 mJ/m^2$), making predictions in the range of observed results (Ohlinger *et al.* 1999). Nucleation rate predicted using this parameter value does not become significant until $SI > 1.8$ (Figure 6). Comparing this interfacial tension assumption to others calculated for struvite above, and to Figure 5, which indicates that significant nucleation occurs for $SI > 0.8$, it appears that this value is too large. In any case, the determined surface tension is only an estimation due to variations in experimental conditions.

3.3.2. Secondary nucleation

Secondary nucleation is said to occur when a crystal is born via any process in which an existing crystal is involved. Many classifications can be made of physical processes leading to secondary nucleation: fracture, needle-breeding, attrition, fluid sheer, and contact nucleation. These are discussed in detail in (Randolph & Larson 1988). Relatively little account is

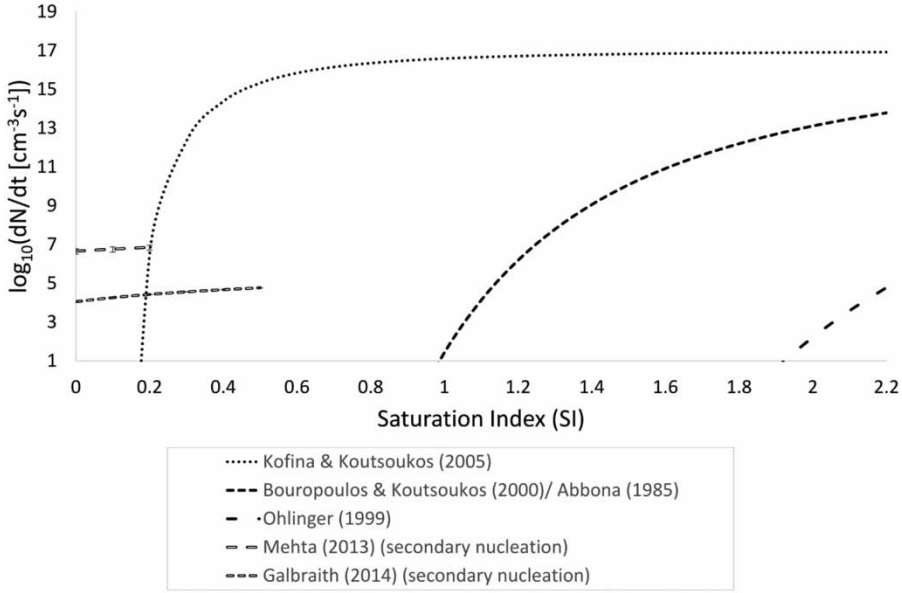

Figure 6 | Nucleation rate model comparison including classic primary nucleation rate models (Kofina & Koutsoukos 2005; Bouropoulos & Koutsoukos 2000; Abbona & Boistelle 1985; Ohlinger *et al.* 1999), and power law models for primary (Galbraith 2011) and secondary (Mehta & Batstone 2013) nucleation.

given to modelling secondary nucleation of struvite, which may play a significant role in crystallisation once a particle population is established. The degree to which each secondary nucleation mechanism occurs (if at all) can depend on particle size, number density, fluid shear, saturation and temperature (Mullin 2001). One study has measured secondary struvite nucleation by measuring particle size distribution (PSD) in batch experiments, seeded with $35 \pm 3\mu m$ struvite particles to ensure that no primary nucleation was possible. The nucleation rate was represented using a power law model (Equation (24)) (Mehta & Batstone 2013).

$$B = \frac{dN}{dt} = k_B(\sigma - \sigma_i)^{n_B} \tag{24}$$

where k_B and n_B are the rate coefficient and exponent, estimated as $8.3 \pm 2.3 \times 10^6$ $[particles \cdot L^{-1}s^{-1}]$ and 1.75 ± 0.13, respectivley, σ_i is the threshold saturation for secondary nucleation, regressed as $\sigma_i = 0.55 \pm 0.1$, which is equivalent to $SI = 0.57 \pm 0.12$. De-supersaturation due to crystal growth was assumed negligible based on an observed 3% reduction in total phosphorus. However, our simulations show that this is equivalent to a 44.18% reduction in supersaturation at the lower supersaturation range, meaning growth likely influenced results. Contact nucleation was proposed as the most likely model, which suggests that particles $< 100\mu m$ do play a significant role in secondary nucleation, contrary to results from previous studies (Larson & Bendig 1976). A similar study operated a seeded laboratory scale crystallizer in the supersaturation range of $SI = 0.25 - 0.79$, assuming mixed suspension mixed product removal (MSMPR) and implemented a general power law model, as shown in Equation (25) (Galbraith *et al.* 2014).

$$B_{nuc} = k_{nuc}SI^{n_{nuc}} \tag{25}$$

where the nucleation rate constant $k_{nuc} = 8.5(\pm 0.076) \times 10^7$ $[particles\ L^{-1}\ min^{-1}]$ and the nucleation rate order $n_{nuc} = 1.68(\pm 0.014)$. Kinetic parameters were regressed by applying a hybrid population balance technique, incorporating nucleation, growth and agglomeration (Galbraith *et al.* 2014).

3.3.3. Struvite nucleation rate model comparison

Figure 6 compares the results of nucleation models applied to struvite crystallisation. Primary nucleation rate is described as a function of *SI*, using multiple estimates of interfacial tension and Equation (22). Equations (24) and (25) are used to describe secondary nucleation.

The primary nucleation rate curves are described over a broad range of saturation index because the interfacial tension is a property which, so far as fundamental theory goes, does not change with supersaturation. Secondary nucleation rate relationships on the other hand are only shown for the saturation range at which their kinetic parameters were calculated since these are empirical relationships. The significant differences in primary nucleation rates resulting from changes in the interfacial tension illustrate how sensitive the model is to this parameter, which is notoriously difficult to estimate.

The asymptotic nature of Equation (22) means that each instance of this model shown in Figure 6 approaches the assumed nucleation rate of $A_n = 1 \times 10^{17} [cm^{-3}s^{-1}]$, although, as shown above, a great deal of uncertainty is also found in this parameter. Secondary nucleation rates are less sensitive to *SI* than primary nucleation rates. Compared to the large variability in primary nucleation rates, results from Mehta and Galbraith are reasonably close, indicating that they are likely a reasonable description of struvite secondary nucleation in that supersaturation range. These results are in the range of 10^4–10^7, which align with rates suggested by Mullin (Mullin 2001), but are significantly different from the assumed primary nucleation pre-exponential factor (10^{17}) and the maximum nucleation rate estimated by Koralewska (in the range of 10^{12}–10^{14}). Unless the transition between primary and secondary nucleation is estimated, and both key parameters in the primary nucleation model are found with a greater degree of certainty, applying a general power law model to nucleation is just as effective as any other method.

3.4. Crystal growth rate

3.4.1. Two-step growth

Particle growth is often described as a two-step process: transport of the solute to the crystal surface and integration from liquid to solid phase on the crystal surface. As these steps must operate in series, the slower of the two is always rate limiting. The dominant mechanism may change depending on the hydrodynamic properties of the system (as investigated by Tai (1999) for sparingly soluble salts), temperature and solution composition (Sohnel & Garside 1992). The two-step model is usually posed as a mass deposition rate but can be converted to a particle linear growth rate with the knowledge of total particle mass, average particle diameter and solution volume (Bhuiyan *et al.* 2008). The diffusion rate can be written as:

$$\frac{dL}{dt} = k_d (C - C_i)^{n_d} \tag{26}$$

where L is particle length/diameter, k_d is the diffusion rate constant, $C - C_i$ is the concentration difference between the bulk solution and the interface, and n_d is the diffusion order, which is almost always assumed to be 1, but may not necessarily be (Mullin 2001). Struvite has been described by the diffusion model when Equation (18) was found to be first order (Ariyanto *et al.* 2014). The surface integration rate, detailed further in the next section, is given as:

$$\frac{dL}{dt} = k_r (C_i - C_{eq})^{n_r} \tag{27}$$

where k_r is the reaction rate constant, $C_i - C_{eq}$ is the concentration difference between the interface and saturation and n_r is the reaction rate order. If $n_r = 1$, the diffusion and reaction steps can be combined to give:

$$\frac{dL}{dt} = K_g (C - C_{eq}) = K_g S \tag{28}$$

For struvite application, the term $(C - C_s)$ should be replaced here by one of the more appropriate descriptions of supersaturation for sparingly soluble salts (generally termed S). In Equation (28), $K_g = k_d k_r / (k_d + k_r)$. Alternatively, if $n_r = 2$, the reaction can be written as:

$$G = \frac{dL}{dt} = k_d S \left[\left(1 + \frac{k_d}{2 k_r S} \right) - \sqrt{\left\{ \left(1 + \frac{k_d}{2 k_r S} \right)^2 - 1 \right\}} \right] \tag{29}$$

Struvite has been modelled using Equation (29), using S_r in place of S, assuming a point distribution of particles and negligible change in seed size (Bhuiyan *et al.* 2008). The number of data points and fit of the model to the data were unclear, shedding some doubt on this work. Both diffusion and growth were considered, and the relative orders of coefficients are used to infer diffusion as the rate controlling mechanism.

3.4.2. Integration controlled growth

After the solute has diffused to the crystal surface, it must be integrated into the crystal lattice. An absorbed layer of solute exists on the surface of a growing crystal. This third phase consists of partially ordered solute in a partially de-solvated lattice. It is not yet crystalline, but it is more ordered and concentrated than the bulk solution. It is the ordering of this layer into a crystalline structure which the integration rate describes.

In many struvite systems (presented later in Table 3), mixing is sufficient to ensure negligible diffusion effects, reducing the growth rate to a surface integration controlled step (Table 3). This step has been described by a number of models. Firstly, a power law model can be used for parameter regression when the form of the growth rate model is unknown. Changes in the growth rate constant and order are then used to infer a more complex model.

$$\frac{dL}{dt} = k_g S^{n_g} \tag{30}$$

where L is the particle length/diameter, k_g is a growth rate constant, S is a general descriptor of supersaturation and n_g is an empirical particle growth rate order. Various works have implemented a form of Equation (30) to describe struvite crystallisation, as detailed in Table 3. Hanhoun regressed nucleation and growth kinetics with a least squares regression, which was predicted by *pH* measurements and a method of moments population balance (Hanhoun *et al.* 2013). Triger investigated struvite growth rate with a least squares regression using measured and predicted turbidity, which accurately predicted PSD properties but not PSD shape (Triger *et al.* 2012). Ali regressed the struvite crystal growth rate, assuming an initial point distribution of particles and performing a least squares regression comparing measured and estimated ammonia, magnesium and phosphorus concentrations and mean crystal size (Ali & Schneider 2008).[7] Galbraith investigated seeded struvite growth rate using a hybrid population balance technique, incorporating nucleation, growth and agglomeration (Galbraith *et al.* 2014). The growth rate regressed exhibited a higher order than the 1–2 traditionally observed for crystallisation ($n_g = 5.062 \pm 0.005$) in the *SI* range of 0.37–0.54. They suggested that the high order could also be represented by a second order model with a dead-zone, where growth rate becomes insignificant below a given supersaturation, SI^*.

$$G = \frac{dL}{dt} = k_g (SI - SI^*)^2 \tag{31}$$

where $SI^* = 0.3$. This outcome reinforces the null supersaturation concept used to describe secondary nucleation (Mehta & Batstone 2013) and the surface nucleation model described in the following (Equation (32).

Two surface integration-based growth mechanisms which have not yet been applied to struvite are the surface nucleation model and the screw dislocation model. The surface nucleation (i.e. birth and spread model) describes nuclei forming on a smooth crystal surface and spreading to sites of lowest energy. In this model, nucleation is the rate controlling step as the spread of nuclei is much faster due to lower energy requirements (Ohara & Reid 1973).

$$G = A' S^p \exp\left(-\frac{B'}{S}\right) \tag{32}$$

where A', B', and p are constants and $p = 1 - 2$. In this equation, B' represents a value of S at which growth becomes significant. When S is significantly larger than B', the exponential term in Equation (32) tends to 1, reducing the equation to the same form as Equation (30). When S is significantly smaller than B', the exponential term (therefore the growth rate) tends to 0. Another alternative is the continuous step growth model, which describes a self-perpetuating kink/dislocation,

[7] Investigations by Ali occurred over a significant time period (36 h), making the operating SI lower than that achieved by the non-equilibrium state of mixing feed streams.

Table 3 | Struvite particle growth rate comparison

Source	pH range[a]	Experimental saturation range as (*SI*)	Phosphate conc. [mM]	Molar ratio Mg: N:P	Reactor type (seeded/ continuous/ batch)	Mixing speed [rpm]	Residence time [min]	Final particle size [μm]	Model equation	Saturation measure	Rate Constant(s) [μm/min]	Rate order presented	Linear growth rate [μm/min]
(Ali & Schneider, 2008)	7.22–7.51	0.053[b]0.32–0.57[c]	6	1:1:1	Seeded fed batch recirculating (16–16.8L)	N/P	439.2, 480 & 2160	~170–195	Power law	SI^a SI^a	0.784 ± 0.14 0.819 ± 0.14	1.64 ± 0.19 1.68 ± 0.18	0.011–0.083(calculated) Power law (Seed size estimated) 0.011–0.07 (calculated)
(Galbraith *et al.* 2014)	7.46–7.62	0.25–0.74	5	1:1:1	Stirred, seeded, draft tube, baffled, batch (1L)	N/P	120	< 30	Power law	*SI*	12.49 ± 0.06	5.062 ± 0.005	0.011–2.74 (calculated)
(Hanhoun *et al.* 2013)	8.5–9.5	0.26–0.54	3–4	1:1:1	Stirred batch (3L)	500	60	D[50] = 70–89	Power law	$IAP^{1/3} - K_{sp}^{1/3}$	280.64	1.34	$2 \times 10^{-4} - 1.3 \times 10^{-3}$ (calculated)
(Ariyanto *et al.* 2014)	8.0–9.5	0.31–1.00	2	1:1:1	Stirred, seeded batch (1 L)	50–120	120	24.3–84.8 (seed size)	Power law	Ω	0.5–10.0	1.05–1.47	0.07–14.39 (calculated)
(Triger *et al.* 2012)	9.31	~3.7[b,d]	14.08 (synth)	1.3:33:1	Stirred batch (2 L)	300	0.33	D[50] = 54.1–52.5	Power law	SI^a	1.75–2	1.15–2	2.72–3.56 (calculated)
	9.29	~3.7[b,d]	14.40 (real)	1.3:19:1	Stirred batch (2 L)	150	0.33	D[50] = 45.7	Power law	SI^a	1.5	1.8	1.98–2.52 (calculated)
	9.29	~3.7[b,d]	13.95 (real)	1.3:16:1	Stirred batch (2 L)	300	0.33	N/P	Power law	SI^a	1.8	2	2.45–3.20 (calculated) 9.35
(Bhuiyan *et al.* 2008)	8.07	< 1.38	~0.7 (read from plot)	N/P	Seeded continuous FBR (5.56 L)	N/P	420	500–2000	Two-step	S_r	$k_d = 1.11 \times 10^{-8}$ $k_r = 7.99 \times 10^{-5}$ [m/s]	2	0.51–16.02 (calculated)
(Mehta & Batstone, 2013)	8.0–9.0	0.12–1.47	3.67	5.14:4.88:1	Stirred, seeded, baffled batch	N/P	120	D[50] ~ 100	Power law (including surface area)	S_r	N/P	N/P	0.02–8.55 (calculated)
(Koralewska *et al.* 2009)	9	4.53–6.59	100–820	1:1:1	Draft tube MSMPR (1.2 L)	6.6	15	< 90	SD RHG	N/P	N/P	N/P	0.03–1.99
(Mazienczuk *et al.* 2012)	9–11	N/P	105	1:1:1	Draft tube MSMPR (1.2 L)	0.25 [W/ kg]	15, 30 & 60	< 90 D[50] = 4.1–19.1	SIG NCG	N/P	N/P	N/P	0.07–0.43
(Kozik *et al.* 2014)	8.5–10	N/P	65	1.2:1:1	DT MSMPR (0.6 L)	4	15, 30 & 60		SIG NCG	N/P	N/P	N/P	0.2–1.0
(Harrison *et al.* 2011)	7.5–8.5	N/P	N/P	N/P	Stirred, seeded batch (1 L)	N/P	N/P	N/P	Power law	ΔC_{PO_4}	N/P	1.9–2.1	10–24
	8.5	N/P	N/P	N/P	Stirred, seeded pilot scale at abattoir (200 L)	N/P	N/P	N/P	Power law	ΔC_{PO_4}	$k_g = 1.5 \times 10^{-5}$ to 1.0 $\times 10^{-4}$ [μm/min/ (mg/L)^2]	2	0.45–0.8

Note: N/P = not provided.

[a]Maximum pH/SI for batch reactors and steady state SI for continuous.

[b]Calculated using thermodynamic model and conditions given.

[c]SI given in PhD thesis document.

[d]High ammonia concentration introduces uncertainty to SI prediction via thermodynamic model.

which forms a screw dislocation. This form of growth has been observed by crystal etching and reflective microscopy (Randolph & Larson 1988). The screw dislocation model is also referred to as Burton Cabrera Frank (BCF) model (Burton *et al.* 1951) and is the most widely applied model.

$$G = A''S^2 \tanh\left(\frac{B''}{S}\right) \tag{33}$$

where A' and B' are constants. At low supersaturations ($S \ll B''$), the hyperbolic term tends towards 1 and the model reduces to a power law with $n_g = 2$. At high supersaturations ($S \gg B''$), the model can be approximated with the power law model with $n_g = 1$. After the proposition of these three model types, it must still be noted that there are scenarios which cannot be explained by any of them (Randolph & Larson 1988).

3.4.3. Growth rate dispersion

Growth rate dispersion (GRD) is an alternative method of describing growth which has been observed in many crystal systems (Randolph & White 1977; Zekic *et al.* 2011; Ochsenbein *et al.* 2015). This phenomenon has been discussed extensively yet remains to be properly understood (Randolph & Larson 1988; Mullin 2001; Mitrović *et al.* 2008; Singh & Ramkrishna 2014). Struvite GRD has been described by the Rojkowski Hyperbolic size-dependent growth model for a MSMPR (Equation (24)), achieving the best fit out of a range of empirical and semi-empirical size-dependent growth models (Matynia *et al.* 2006; Koralewska *et al.* 2009; Lobanov 2009). While this model may provide the best fit to some data, it was not compared to size-independent growth models and there is no physical evidence that size-dependent growth is occurring, making it as good as any other that could be fit to the same data.

$$n(L) = n_0 \exp\left[-\left(\frac{G_\infty - G_0}{\tau a G_\infty^2}\ln\left(\frac{aG_\infty L + G_0}{G_0}\right) + \frac{L}{\tau G_\infty} + \ln\left(\frac{aG_\infty L + G_0}{(1+aL)G_0}\right)\right)\right] \tag{34}$$

where $n(L)$ is the population density [particles m^{-1} m^{-3}], n_0 is the nuclei population density [particles m^{-1} m^{-3}], a is a kinetic coefficient [m^{-1}], τ is the mean residence time of a crystalliser working volume [s^{-1}] and G_0 [m s^{-1}] and G_∞ [m s^{-1}] are the growth rates of the nuclei and the largest crystals, respectively.

3.4.4. Struvite growth rate model comparison

In this section, struvite research is evaluated to identify struvite growth rate trends and assess which practices should and should not be adopted.[8] Table 3 summarises struvite crystallisation investigations and Figure 7 provides a visual comparison of crystal growth rates on a common supersaturation scale. Table 3 shows that the measured struvite crystal growth rate is reported from 0.03 to 24 μm/min, while regressions based on Figure 7 showed growth rates of 0.01–12.86 μm/min in the *SI* range of 0.25–1.4. Unfortunately, such a large range in growth rate does not offer much confidence for accurate design purposes. The impact of uncertainty on process design should be examined by conducting sensitivity analysis on struvite crystallisation kinetic parameters.

Comparison of growth rates predicted by kinetic models at differing experimental conditions shows no major trends (Figure 7). This figure shows that growth rates predicted by different models vary over five orders of magnitude. It appears that seeded system's growth rates are much higher than unseeded ones, although further unseeded investigations are necessary to validate this trend. All authors reported increasing crystal growth rate with *SI* except Kozik and Mazienczuk, who observed a decrease in growth rate with increasing pH[9], which can be attributed to a greater initial nucleation rate and associated decrease in *SI*. Large variation in Figure 7 can be explained by assumptions, experimental techniques and regression techniques, all of which are detailed in the following.

A key assumption in many growth rate models is negligible nucleation and agglomeration. This is supported by the assumption of a fixed distribution of particles (Ali & Schneider 2008; Bhuiyan *et al.* 2008). This fixed distribution has been assumed to be a point distribution which does not change in size (Bhuiyan), or a measured mean particle size which does

[8] Species depletion models are not considered adequate for struvite modelling because of the relationship observed between rate constant and ion concentrations (section 3.2)

[9] SI is proportional to under the conditions tested

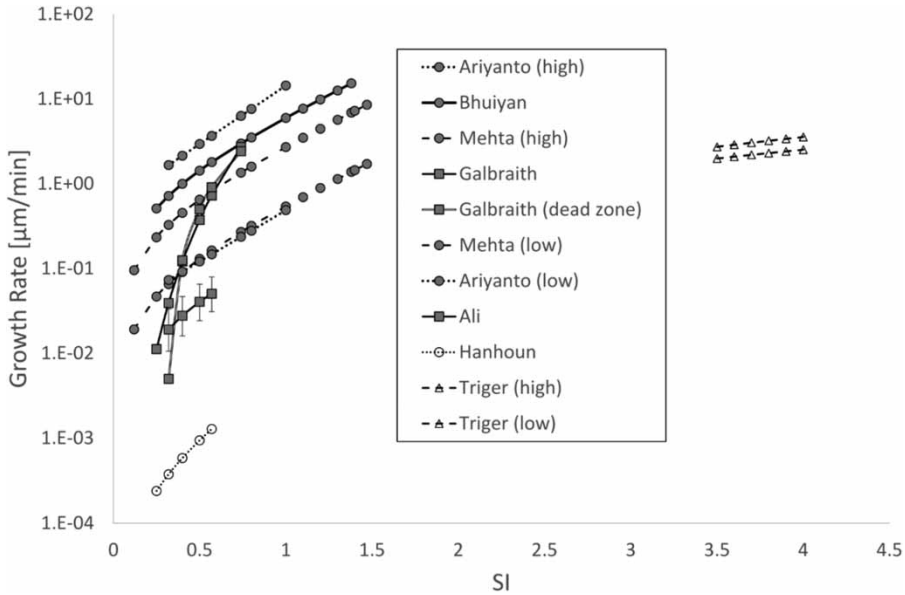

Figure 7 | Crystal linear growth rate comparison. Dashed and solid lines represent batch and continuous reactors, respectively. Circles indicate $C_{PO_4} < 5$ mM, squares indicate 5 mM $\leq C_{PO_4} <$ 10 mM and triangles indicate $C_{PO_4} \geq 10$ mM. Filled and unfilled markers represent seeded and unseeded scenarios, respectively. Uncertainties in kinetic parameters were incorporated where available and significant enough to be visible.

(Ali & Schneider 2008). Alternatively, researchers have assumed constant *PSD* shape and calculated growth rate using *PSD* translation (Harrison *et al.* 2011; Ariyanto *et al.* 2014). Harrison's results must be taken cautiously though as they showed that *PSD* shape did vary and represented supersaturation using phosphorus concentration difference, neglecting ion speciation. A final technique used to assume negligible struvite nucleation and aggregation has been to incorporate a specific surface area term (measured) rather than assuming a point distribution (Mehta & Batstone 2013). By converting from the molar growth rate, they estimated crystal linear growth rate to be 0.06–0.3 µm/min/unit of S_r in the *SI* range of 0.12–1.47, although PSD assumptions necessary to make this conversion were unclear. The corresponding maximum and minimum crystal growth rates span a significant range but are within the region of growth rates predicted by another research (Figure 7). Although each of the abovementioned growth only models were able to produce a good fit to their individual datasets, the growth rate predictions vary by two orders of magnitude (Figure 7). The next steps in model complexity are to use full PSD measurements for regressions and include the nucleation mechanism.

Multiple works have modelled simultaneous struvite nucleation and growth using population balance techniques. Investigations by Triger incorporate nucleation and growth but regressed parameters using only turbidity (Triger *et al.* 2012). Their experiments were conducted at a very high *SI*, but growth rates regressed were in line with other works at lower *SI* values, indicating a diffusion limitation. The authors attribute errors to non-ideal mixing and attrition, although agglomeration and operation at a very high *SI* may also play a role. Hanhoun also applied a nucleation and crystal growth model, but manually selected nucleation parameters, and while a least squares regression was used, it was only applied to saturation data predicted from pH rather than concentration or PSD data (Hanhoun *et al.* 2013). This resulted in a growth rate prediction significantly lower than those of other struvite investigations (Figure 7), which suggests that a single variable is insufficient for parameter estimation. Koralewska incorporated nucleation and growth mechanisms and used a highly controlled procedure, giving reasonable confidence to the range of particle growth rates they measured, although the growth rate dispersion model they applied is theoretically unlikely, as discussed earlier (Koralewska *et al.* 2009). Work by Mazienczuk and Kozic regressed nucleation and growth parameters using the PSD only (Mazienczuk *et al.* 2012; Kozik *et al.* 2014). While their work was experimentally sound, the model proposed should be applied cautiously as it did not match the data in lower particle size ranges, indicating that the nucleation and growth model alone could not accurately represent the entire dataset. Improvements in these works include: (1) making regressions using multiple variables, (2) not operating at a high *SI* and (3) examining agglomeration (discussed in the following).

Many authors suggest that since the order of reaction regressed is >1, crystallisation is likely reaction controlled. The texts often cited to justify this conclusion measure supersaturation in the diffusion-reaction model using a difference in solute

concentration (Randolph & Larson 1988; Mullin 2001). Most investigations of struvite use one of various more complex descriptions of supersaturation, the selection of which will result in a variation in regressed model order. In addition to this, Mullin notes that diffusion and integration are difficult to distinguish considering that likely more steps are involved (i.e. boundary layer, adsorption layer and surface diffusion, ion dehydration, surface integration and counter diffusion of dehydrated water) and that diffusion term may exhibit a higher order than 1.

To examine the effect of supersaturation measure on regressed growth rate order, a power law model using *SI* was fit to each trend shown in Figure 7. All models gave an R^2 value >0.97 and the indices varied from 1.64 to 2 for all models except that by Galbraith *et al.*, which has an order of 5.062. By repeating this process using reduced saturation, it was found that growth rate orders mostly fell in the range of 0.9–1.34, while results from Triger *et al.* and Galbraith *et al.* gave orders of 0.21–0.23 and 3.14, respectively. In this case, all R^2 values were >0.99. This illustrates that great care must be taken to ensure consistency between the selection of supersaturation measures and that conclusions about reaction or diffusion mechanisms must be taken cautiously.

3.5. Aggregation

3.5.1. Aggregation theory

Smoluchowski originally described the collision frequency of dispersed particles due to Brownian motion (Smoluchowski 1917). A general expression of aggregation describes the rate of aggregation (r_{agg}) of particles of size i with those of size j as proportional to the product of the number of particles in each size range (N_i and N_j) and includes a rate constant known as the aggregation kernel, $\beta_{i,j}$.

$$r_{agg} = \beta_{i,j} N_i N_j \tag{35}$$

The aggregation kernel can be broken down into two terms: β_0, representing system properties (supersaturation, and fluid velocity), and a particle size-dependent function, $f(i, j)$, representing the aggregation frequency. The size dependence term can take various forms depending on the mechanism(s) causing aggregation (perikinetic and orthokinetic). Aggregation investigations are notoriously difficult because of the many concurrent influencing factors. In the century since Smoluchowski's formulation, many investigations have been made into the agglomeration kernel and now more than 50 variants of the agglomeration kernel can be found in the literature (Hounslow 1990; Bramley 1994; Mersmann *et al.* 2002).

Although many aggregation investigations have been made, fewer investigations have been made into the struvite system. Therefore, before presenting investigations into struvite, a similar sparingly salt system is used here to discuss the relevant theory: calcium oxalate monohydrate (COM). For COM aggregation has been investigated for dependency on a number of factors including: hydrodynamics (Bramley *et al.* 1997; Hounslow *et al.* 1998); solution composition (Hounslow *et al.* 1998); Thiele modulus (a term describing the ratio of reaction rate to diffusion rate) (Hounslow *et al.* 1998); and solution ionic ratio (Bramley *et al.* 1997; Liew *et al.* 2003). It was found that a maximum aggregation rate exists with varying shear rates, due to a trade-off between increasing collision rate and increasing tensile stress between crystals (Mumtaz *et al.* 1997). All of the abovementioned factors were able to be correlated by comparing particle collision efficiency with a number representing the ratio of aggregate bond strength of an aggregate to the force exerted on it in a collision (Hounslow *et al.* 2001). Similar theoretical collision efficiency models have been developed incorporating hydrodynamic and colloidal interactions, accounting for particle mass, fractal dimension and a non-dimensional Hamaker constant (Babler 2008)[10]. Babler's work concluded that collisions between particles of similar size are preferential to those with different sizes. This outcome is of importance in crystallisation applications as often it is assumed that particle surface area is not conserved during aggregation events, and that the effect of this assumption is relatively low because the majority of collisions occur between particles of significantly different sizes.

While it is physically accurate that aggregation mechanisms depend on particle size, the overall aggregation kernel can often be approximated by a size-independent kernel (Jones 2002). In a number of investigations, a size-independent kernel has provided a better fit to data than size-dependent kernels (Hounslow 1990; Ilievski 1991; Bramley 1994). This outcome has been attributed to a decrease in collision efficiency and increased particle disruption with particle size (Jones 2002). In this scenario, the aggregation rate becomes a function of hydrodynamics and supersaturation only. For a size-independent

[10] Application to crystallisation systems would likely also require a description of the growth rate of a bridging bond.

system where hydrodynamics remain constant, the aggregation kernel can be modelled using a simple power law model (Equation (36)), where the saturation index (SI) is the driving force, k_{agg} and n_{agg} are the rate constant and order, respectively.

$$\beta_{i,j} = \beta_0 = k_{agg}(SI)^{n_{agg}} \tag{36}$$

3.5.2. Struvite aggregation

Early work on struvite crystallisation showed that for equimolar solutions of magnesium, ammonium and phosphate, twinning and aggregation occurs above a concentration of approximately 0.004 M, where the supersaturation necessary for aggregation is approximately $SI = 1.51$, but progressively decreases with increasing concentration (Abbona & Boistelle 1985). Struvite aggregation is evident in microscopy from multiple scenarios (Battistoni *et al.* 2005; Huang *et al.* 2006), and other fluidised bed reactors (FBR) have generated particle sizes of 0.41–1.43 mm (Shimamura *et al.* 2003) and 2.2–3.5 mm (Adnan *et al.* 2003), which are likely only achieved by aggregation. Another FBR investigation observed pellets with a tightly bound inner core and a thick outside coating of fines (Bhuiyan & Mavinic 2008).

In addition to struvite crystallisation, one group observed 2–3 μm hydroxyapatite agglomerates forming both alone and on the surface of struvite crystals (Hutnik *et al.* 2011). While struvite aggregation is commonly observed, it is not yet thoroughly investigated. Only one work which experimentally determined kinetics of struvite nucleation, growth and aggregation (Galbraith *et al.* 2014). Discretised population balance methods were used to analyse data from a stirred batch vessel fed with equimolar 0.005 M feed operating at $SI = 0.37$–0.74. Galbraith used Equation (22) to find an aggregation kernel in the range of 10^{-8} to 10^{-10}, which was within a reasonable range when compared to studies of other sparingly soluble salts. While that work regresses kinetic parameters using extensive PSD and concentration data, it does find a high correlation between kinetic parameters and makes assumptions about the PSD below 2 μm. Future publications by our research group will detail nucleation, growth and aggregation kinetic parameter optimisations using experimental data from a Poiseuille flow reactor (Burns *et al.* 2016).

4. CONCLUSIONS AND RECOMMENDATIONS

Modelling of thermodynamics to simulate saturation and other relevant variables, such as elemental concentration in the liquid phase and struvite mass, showed close agreement with collected data only when specific equilibrium databases were used. Assessing Davies and Samson activity models show an atypical trend in the activity coefficients to be aware of, but the application of either of them at ionic strength below 0.5 M can still provide reliable information. Selection of different equilibrium equations in PHREEQC databases can provide high variability in the predicted struvite SI, suggesting that equilibrium simulations are only comparable when detail of the equilibrium datasets are provided. Simulations developed with several equilibrium databases show that 'sit' is most suitable for rapid estimations in struvite precipitation. However, the development of a targeted thermodynamic model produces the most reliable results.

The author's own model in EES was tested in struvite precipitation experiments to discuss an expected variability in a real digested liquor solution, showing that equilibrium and non-equilibrium calculations can predict laboratory measurements. In this context, prediction variability will depend on the quantity of entry data and thermodynamic parameters. Additionally, the same model was tested against several struvite batch precipitation, showing high proximity when the elemental concentration of P and Mg in the desaturated solution were compared.

Comparison of studies showed that struvite induction time increases exponentially below $SI = 0.8$ and that the lower saturation limit for homogeneous nucleation occurs in the range of $SI = 0.237$–0.69. Struvite primary nucleation rate is highly sensitive to interfacial tension and due to the high uncertainty in primary and secondary nucleation kinetic model and in the transition between primary and secondary nucleation, a power law model may be equally as effective at describing nucleation.

Estimated struvite growth rates vary over five orders of magnitude, limiting inferences which could be drawn. However, growth rates were consistently higher under conditions using seed particles. Exponentially decaying growth rates at low supersaturation indicated that a surface nucleation model might be suitable for future struvite growth investigations. Comparison of struvite growth models highlighted the influence of saturation description on estimated rate order, showing that rate order cannot be accurately used to infer crystal growth mechanism. Overall, more consistent results are required to develop a functional predictive kinetic model for struvite crystallisation. Uncertainty in results can be reduced by (1) applying kinetic

models which fully describe crystallisation mechanisms (nucleation, growth, aggregation); (2) using large datasets including full *PSD* measurements; and (3) performing model regressions using multiple variables.

ACKNOWLEDGEMENTS

We would like to acknowledge the College of Science and Engineering at James Cook University for providing research support funding.

DATA AVAILABILITY STATEMENT

All relevant data are included in the paper or its Supplementary Information.

CONFLICT OF INTEREST

The authors declare there is no conflict.

REFERENCES

Abbona, F. & Boistelle, R. 1985 Nucleation of struvite ($MgNH_4PO_4.6H_2O$) single crystals and aggregates. *Crystal Research and Technology* **20** (2), 133–140.

Adnan, A., Mavinic, D. S. S. & Koch, F. A. A. 2003 Pilot-scale struvite recovery from anaerobic digester supernatant at an enhanced biological phosphorus removal wastewater treatment plant. *Journal of Environmental Engineering and Science* **2**, 315–324.

Ali, M. I. 2007 Struvite crystallization in fed-batch pilot scale and description of solution chemistry of struvite. *Chemical Engineering Research and Design* **85** (3), 344–356. https://doi.org/10.1205/cherd06031.

Ali, M. I. & Schneider, P. A. 2008 An approach of estimating struvite growth kinetic incorporating thermodynamic and solution chemistry, kinetic and process description. *Chemical Engineering Science* **63** (13), 3514–3525.

APHA 1999 *Standard Methods for the Examination of Water and Wastewater-Part 1000 Standard Methods for the Examination of Water and Wastewater*. American Public Health Association, Washington, DC, USA.

Ariyanto, E., Sen, T. K. & Ang, H. M. 2014 The influence of various physico-chemical process parameters on kinetics and growth mechanism of struvite crystallisation. *Advanced Powder Technology* **25** (2), 682–694.

Babić-Ivančić, V., Kontrec, J., Kralj, D. & Brečević, L. 2002 Precipitation diagrams of struvite and dissolution kinetics of different struvite morphologies. *Croatica Chemica Acta* **75** (1), 89–106.

Babić-Ivancić, V., Kontrec, J., Brecević, L. & Kralj, D. 2006 Kinetics of struvite to newberyite transformation in the precipitation system $MgCl_2$-$NH_4H_2PO_4$NaOH-H_2O. *Water Research* **40** (18), 3447–3455. https://doi.org/10.1016/j.watres.2006.07.026.

Babler, M. U. 2008 A collision efficiency model for flow-induced coagulation of fractal aggregates. *AIChE* **54** (7), 1748–1760. https://doi.org/10.1002/aic.

Barnes, N. J. & Bowers, A. R. 2017 A probabilistic approach to modeling struvite precipitation with uncertain equilibrium parameters. *Chemical Engineering Science* **161**, 178–186. https://doi.org/10.1016/j.ces.2016.12.026.

Barsanti, K. C., McMurry, P. H. & Smith, J. N. 2009 The potential contribution of organic salts to new particle growth. *Atmospheric Chemistry and Physics* **9** (9), 2949–2957. https://doi.org/10.5194/acp-9-2949-2009.

Battistoni, P., Paci, B., Fatone, F. & Pavan, P. 2005 Phosphorus removal from supernatants at low concentration using packed and fluidized-bed reactors. *Industrial & Engineering Chemistry Research* **44**, 6701–6707.

Bhuiyan, M. I. H. & Mavinic, D. S. 2008 Assessing struvite precipitation in a pilot-scale fluidized bed crystallizer. *Environmental Technology* **29** (11), 1157–1167. https://doi.org/10.1080/09593330802075452.

Bhuiyan, M. I. H., Mavinic, D. S., Beckie, R. D., Bhuiyan, M., Beckie, D. S., Bhuiyan, R. D., Mavinic, M. I. H., Beckie, D. S., Bhuiyan, R. D., Mavinic, D. S., Beckie, R. D., Bhuiyan, M. I. H., Mavinic, D. S. & Beckie, R. D. 2007 A solubility and thermodynamic study of struvite. *Environmental Technology* **28** (9), 1015–1026. https://doi.org/10.1080/09593332808618857.

Bhuiyan, M., Iqbal, H., Mavinic, D. S. & Beckie, R. D. 2008 Nucleation and growth kinetics of struvite in a fluidized bed reactor. *Journal of Crystal Growth* **310** (6), 1187–1194. https://doi.org/10.1016/j.jcrysgro.2007.12.054.

Bhuiyan, M. I. H., Mavinic, D. S. & Beckie, R. D. 2009 Dissolution kinetics of struvite pellets grown in a pilot-scale struvite crystallizer. *Canadian Journal of Civil Engineering* **36**, 550–558.

Bouropoulos, N. C. & Koutsoukos, P. G. 2000 Spontaneous precipitation of struvite from aqueous solutions. *Journal of Crystal Growth* **213** (3–4), 381–388.

Bramley, A. S. 1994 *A Study of the Growth and Aggregation of Calcium Oxalate Monohydrate.* PhD thesis, University of Adelaide, Adelaide, Australia.

Bramley, A., Hounslow, M. & Ryall, R. 1997 Aggregation during precipitation from solution. kinetics for calcium oxalate monohydrate. *Chemical Engineering Science* **52** (5), 747–757.

Bromley, L. A. 1974 Thermodynamic properties of strong electrolytes in aqueous solutions. *AIChE Journal* **19** (2), 313–320.

Buchanan, J. R., Mote, C. R. & Robinson, R. B. 1994 Thermodynamics of struvite formation. *Transactions American Society Agricultural Engineers* **37** (2), 617–621.

Burns, M., Natividad Marin, L. & Schneider, P. A. 2016 Investigations of a continuous Poiseuille flow struvite seed crystallizer – mixer performance and aggregate disruption by sonication. *Chemical Engineering Journal* **295**, 552–562. https://doi.org/10.1016/j.cej.2016.03.061.

Burns, M., Sheehan, M. & Schneider, P. A. 2021 Nucleation and crystal growth kinetic parameter optimization of a continuous Poiseuille flow struvite crystallizer using a discretized population balance and dynamic fluid model. *Chemical Engineering Journal* **405** (June 2020), 126607. https://doi.org/10.1016/j.cej.2020.126607.

Burton, W. K., Cabrera, N. & Frank, N. C. 1951 The growth of crystals and the equilibrium structure of their surfaces. *Philosophical Transactions* **A243**, 299–358.

Capdevielle, A., Sykorova, E., Biscans, B., Beline, F. & Daumer, M. 2013 Optimization of struvite precipitation in synthetic biologically treated swine wastewater – Determination of the optimal process parameters. *Journal of Hazardous Materials* **244–245**, 357–369. http://dx.doi.org/10.1016/j.jhazmat.2012.11.054

Cooper, J., Lombardi, R., Boardman, D. & Carliell-Marquet, C. 2011 The future distribution and production of global phosphate rock reserves. *Resources, Conservation and Recycling* **57** (January), 78–86. https://doi.org/10.1016/j.resconrec.2011.09.009.

Demeestere, K., Smet, E., Van Langenhove, H. & Galbacs, Z. 2001 Optimalisation of magnesium ammonium phosphate precipitation and its applicability to the removal of ammonium. *Environmental Technology* **22** (12), 1419–1428. https://doi.org/10.1080/09593332208618177.

Elduayen-Echave, B., Lizarralde, I., Schneider, P. A., Ayesa, E., Larraona, G. S. & Grau, P. 2021 Inclusion of shear rate effects in the kinetics of a discretized population balance model: application to struvite precipitation. *Water Research* **200**, 117242. https://doi.org/10.1016/j.watres.2021.117242.

Fattah, K. P., Mavinic, D. S., Koch, F. A. & Jacob, C. 2008 Determining the feasibility of phosphorus recovery as struvite from filter press centrate in a secondary wastewater treatment plant. *Journal of Environmental Science and Health Part A, Toxic/Hazardous Substances & Environmental Engineering* **43** (7), 756–764.

Fevotte, G., Gherras, N. & Moutte, J. 2013 Batch cooling solution crystallization of ammonium oxalate in the presence of impurities: study of solubility, supersaturation, and steady-state inhibition. *Crystal Growth and Design* **13** (7), 2737–2748. https://doi.org/10.1021/cg301737s.

Gadekar, S. & Pullammanappallil, P. 2009 Validation and applications of a chemical equilibrium model for struvite precipitation. *Environmental Modeling & Assessment* **15** (3), 201–209.

Galbraith, S. C. 2011 *A Study of Struvite Nucleation, Crystal Growth and Aggregation (Issue November)*.

Galbraith, S. C. & Schneider, P. A. 2009 A review of struvite nucleation studies. *International Conference on Nutrient Recovery* **1**, 69–78.

Galbraith, S. C. & Schneider, P. A. 2014 Modelling and simulation of inorganic precipitation with nucleation, crystal growth and aggregation: a new approach to an old method. *Chemical Engineering Journal* **240**, 124–132. https://doi.org/10.1016/j.cej.2013.11.070.

Galbraith, S. C., Schneider, P. A. & Flood, A. E. 2014 Model-driven experimental evaluation of struvite nucleation, growth and aggregation kinetics. *Water Research* **56C**, 122–132. https://doi.org/10.1016/j.watres.2014.03.002.

Golubev, S. V., Pokrovsky, O. S. & Savenko, V. S. 2001 Homogeneous precipitation of magnesium phosphates from seawater solutions. *Journal of Crystal Growth* **223**, 550–556.

Hanhoun, M., Montastruc, L., Azzaro-Pantel, C., Biscans, B., Frèche, M. & Pibouleau, L. 2011 Temperature impact assessment on struvite solubility product: a thermodynamic modeling approach. *Chemical Engineering Journal* **167** (1), 50–58.

Hanhoun, M., Montastruc, L., Azzaro-Pantel, C., Biscans, B., Frèche, M. & Pibouleau, L. 2013 Simultaneous determination of nucleation and crystal growth kinetics of struvite using a thermodynamic modeling approach. *Chemical Engineering Journal* **215–216**, 903–912. https://doi.org/10.1016/j.cej.2012.10.038.

Harada, H., Shimizu, Y., Miyagoshi, Y., Matsui, S., Matsuda, T. & Nagasaka, T. 2006 Predicting struvite formation for phosphorus recovery from human urine using an equilibrium model. *Water Science and Technology* **54** (8), 247–255. https://doi.org/10.2166/wst.2006.720.

Harrison, M. L., Johns, M. R., White, E. T. & Mehta, C. M. 2011 Growth rate kinetics for struvite crystallisation. *Chemical Engineering Transactions* **25**, 309–314.

Hounslow, M. J. 1990 *A Discretized Population Balance for Simultaneous Nucleation, Growth and Aggregation*. University of Adelaide, Adelaide, South Australia.

Hounslow, M. J., Bramley, A. S. & Paterson, W. R. 1998 Aggregation during precipitation from solution. A pore diffusion – reaction model for calcium oxalate monohydrate. *Water* **391** (203), 383–391.

Hounslow, M., Mumtaz, H., Collier, A., Barrick, J. & Bramley, A. 2001 A micro-mechanical model for the rate of aggregation during precipitation from solution. *Chemical Engineering Science* **56** (7), 2543–2552.

Huang, H., Mavinic, D. S., Lo, K. V. & Koch, F. A. 2006 Production and basic morphology of struvite crystals from a pilot-scale crystallization process. *Environmental Technology* **27** (3), 233–245. https://doi.org/10.1080/09593332708618637.

Hutnik, N., Piotrowski, K., Wierzbowska, B. & Matynia, A. 2011 Continuous reaction crystallization of struvite from phosphate (V) solutions containing calcium ions. *Evolution* **449** (5), 443–449. https://doi.org/10.1002/crat.201100049.

Ilievski, D. 1991 *Modelling Al(OH)3 Agglomeration During Batch and Continuous Precipitation in Supersaturated Caustic Aluminate Solutions*. PhD thesis, University of Queensland, Brisbane, Australia.

Iqbal, M., Bhuiyan, H. & Mavinic, D. S. 2008 Assessing struvite precipitation in a pilot-scale fluidized bed crystallizer. *Environmental Technology* **29** (11), 1157–1167. https://doi.org/10.1080/09593330802075452.

Jia, G., Zhang, H., Krampe, J., Muster, T., Gao, B., Zhu, N. & Jin, B. 2017 Applying a chemical equilibrium model for optimizing struvite precipitation for ammonium recovery from anaerobic digester effluent. *Journal of Cleaner Production* **147**, 297–305. https://doi.org/10.1016/j.jclepro.2017.01.116.

Jones, A. G. 2002 *Crystallization Process Systems (First)*. Heinemann, Butterworth, Oxford, UK.

Kabdasli, I., Parsons, S. A. & Tunay, O. 2006 Effect of major ions on induction time of struvite precipitation. *Croatia Chemica ACTA* **79** (2), 243–251.

Kataki, S., West, H., Clarke, M. & Baruah, D. C. 2016 Phosphorus recovery as struvite: recent concerns for use of seed, alternative Mg source, nitrogen conservation and fertilizer potential. *Resources, Conservation and Recycling* **107**, 142–156. https://doi.org/10.1016/j.resconrec.2015.12.009.

Kofina, A. N. & Koutsoukos, P. G. 2005 Spontaneous precipitation of struvite from synthetic wastewater solutions. *Crystal Growth & Design* **5** (2), 489–496. https://doi.org/10.1021/cg049803e.

Koralewska, J., Piotrowski, K., Wierzbowska, B. & Matynia, A. 2009 Kinetics of reaction-crystallization of struvite in the continuous draft tube magma type crystallizers-influence of different internal hydrodynamics. *Chinese Journal of Chemical Engineering* **17** (2), 330–339. https://doi.org/10.1016/S1004-9541(08)60212-8.

Kozik, A., Hutnik, N., Piotrowski, K. & Matynia, A. 2014 Continuous reaction crystallization of struvite from diluted aqueous solution of phosphate(V) ions in the presence of magnesium ions excess. *Chemical Engineering Research and Design* **92** (3), 481–490. https://doi.org/10.1016/j.cherd.2013.08.032.

Larson, M. A. & Bendig, L. L. 1976 Nuclei generation from repetitive contacting. *AIChE Symposium Series* **72** (153), 21–27.

Laxson, W. W. & Finke, R. G. 2014 Nucleation is second order: an apparent kinetically effective nucleus of two for Ir(0)n nanoparticle formation from IrI·P2W15Nb3O62]8− plus hydrogen. *Journal of the American Chemical Society* **136**, 17601–17615.

Le Corre, K. S., Valsami-Jones, E., Hobbs, P. & Parsons, S. A. 2007 Kinetics of struvite precipitation: effect of the magnesium dose on induction times and precipitation rates. *Environmental Technology* **28** (12), 1317–1324.

Liew, B. T. L., Barrick, J. P. & Hounslow, M. J. 2003 A micro-mechanical model for the rate of aggregation during precipitation from solution. *Chemical Engineering & Technology* **26** (3), 282–285.

Liu, J. C. & Warmadewanthi, I. D. A. A. 2009 Recovery of phosphate and ammonium as struvite from semiconductor wastewater. *Separation and Purification Technology* **64**, 368–373.

Liu, B., Giannis, A., Zhang, J., Chang, V. W.-C. & Wang, J.-Y. 2013 Characterization of induced struvite formation from source-separated urine using seawater and brine as magnesium sources. *Chemosphere* **93** (11), 2738–2747.

Lizarralde, I., Fernández-Arévalo, T., Brouckaert, C., Vanrolleghem, P., Ikumi, D. S., Ekama, G. A., Ayesa, E. & Grau, P. 2015 A new general methodology for incorporating physico-chemical transformations into multiphase wastewater treatment process models. *Water Research* **74**, 239–256. https://doi.org/10.1016/j.watres.2015.01.031.

Lobanov, S. 2009 Struvite reaction-crystallisation as applied to wastewater treatment technology to remove ammonium ions. In *International Conference on Nutrient Recovery From Wastewater Streams*, IWA Publishing, London, UK.

Martín-Hernández, E., Ruiz-Mercado, G. J. & Martín, M. 2020 Model-driven spatial evaluation of nutrient recovery from livestock leachate for struvite production. *Journal of Environmental Management* **271** (June), 110967. https://doi.org/10.1016/j.jenvman.2020.110967.

Matynia, A., Koralewska, J. & Wierzbowska, B. 2006 The influence of process parameters on struvite continuous crystallization kinetics. *Chemical Engineering Communications* **193** (2001), 160–176. https://doi.org/10.1080/009864490949008.

Mazienczuk, A., Matynia, A., Piotrowski, K. & Wierzbowska, B. 2012 Reaction crystallization of struvite in a continuous draft tube magma (DTM) crystallizer with a jet pump driven by recirculated mother solution. *Procedia Engineering* **42** (August), 1540–1551. https://doi.org/10.1016/j.proeng.2012.07.547.

Mehta, C. M. & Batstone, D. J. 2013 Nucleation and growth kinetics of struvite crystallization. *Water Research* **47** (8), 2890–2900. https://doi.org/10.1016/j.watres.2013.03.007.

Mehta, C. M., Khunjar, W. O., Nguyen, V., Tait, S. & Batstone, D. J. 2014 Technologies to recover nutrients from waste streams: a critical review. *Critical Reviews in Environmental Science and Technology* **45** (4), 385–427. https://doi.org/10.1080/10643389.2013.866621.

Mersmann, A., Braun, B. & Löffelmann, M. 2002 Prediction of crystallization coefficients of the population balance. *Chemical Engineering Science* **57** (20), 4267–4275. https://doi.org/10.1016/S0009-2509(02)00343-3.

Mitrović, M. M. M., Žekić, A. a. A. & Baroš, Z. Z. Z. 2008 Growth rate changes of sodium chlorate crystals independent of growth conditions. *Chemical Physics Letters* **464** (1–3), 38–41. https://doi.org/10.1016/j.cplett.2008.08.104.

Morales, N., Boehler, M. A., Buettner, S., Liebi, C. & Siegrist, H. 2013 Recovery of N and P from urine by struvite precipitation followed by combined stripping with digester sludge liquid at full scale. *Water* **5**, 1262–1278.

Mousavi, S. E., Choudhury, M. R. & Rahaman, M. S. 2019 3-D CFD-PBM coupled modeling and experimental investigation of struvite precipitation in a batch stirred reactor. *Chemical Engineering Journal* **361** (November 2018), 690–702. https://doi.org/10.1016/j.cej.2018.12.089.

Mullin, J. W. 2001 *Crystallization* (pp. 1–63). https://doi.org/10.1002/0471238961.0318251918152119.a01.pub3.

Mumtaz, H., Hounslow, M., Seaton, N. & Paterson, W. 1997 Orthokinetic aggregation during precipitation: a computational model for calcium oxalate monohydrate. *Chemical Engineering Research and Design* **75** (2), 152–159.

Musvoto, E. 2000 Integrated chemical-'physical processes modelling-'II. simulating aeration treatment of anaerobic digester supernatants. *Water Research* **34** (6), 1868–1880. https://doi.org/10.1016/S0043-1354(99)00335-8.

Nelson, N. O., Mikkelsen, R. L. & Hesterberg, D. L. 2003 Struvite precipitation in anaerobic swine lagoon liquid: effect of pH and Mg:P ratio and determination of rate constant. *Bioresource Technology* **89** (3), 229–236.

Nordstrom, D. K., Plummer, L. N., Langmuir, D., Busenberg, E., May, H. M., Jones, B. F. & Parkhurst, D. L. 1990 Revised chemical equilibrium data for major water-mineral reactions and their limitations. In: *Chemical Modeling of Aqueous Systems II: American Chemical Society Symposium Series 416* (Melchior, D. C. & Bassett, R. L., eds). American Chemical Society, Los Angeles, CA, USA, pp. 399–413.

Ochsenbein, D. R., Schorsch, S., Salvatori, F., Vetter, T., Morari, M. & Mazzotti, M. 2015 Modeling the facet growth rate dispersion of β l-glutamic acid – combining single crystal experiments with nD particle size distribution data. *Chemical Engineering Science* **133**, 30–43. https://doi.org/10.1016/j.ces.2015.02.026.

Ohara, M. & Reid, R. C. 1973 *Modeling Crystal Growth Rates From Solution*. Prentice-Hall, New Jersey, USA.

Ohlinger, K. N., Young, T. M. & Schroeder, E. D. 1998 Predicting struvite formation in digestion. *Water Research* **32** (12), 3607–3614.

Ohlinger, K. N., Young, T. M. & Schroeder, E. D. 1999 Kinetics effects on preferential struvite accumulation in wastewater. *Journal of Environmental Engineering* **125** (8), 730–737.

Ohlinger, K. N., Young, T. M. & Schroeder, E. D. 2000 Postdigestion struvite precipitation using a fluidized bed reactor. *Journal of Environmental Engineering* **126** (4), 361–368.

Pastor, L., Mangin, D., Barat, R. & Seco, A. 2008 A pilot-scale study of struvite precipitation in a stirred tank reactor : conditions influencing the process. *Bioresource Technology* **99**, 6285–6291.

Quintana, M., Sánchez, E., Colmenarejo, M. F., Barrera, J., García, G. & Borja, R. 2005 Kinetics of phosphorus removal and struvite formation by the utilization of by-product of magnesium oxide production. *Chemical Engineering Journal* **111** (1), 45–52.

Rahaman, M. S., Ellis, N. & Mavinic, D. S. 2008 Effects of various process parameters on struvite precipitation kinetics and subsequent determination of rate constants. *Water Science and Technology* **57** (5), 647–654.

Randolph, A. & Larson, M. 1988 Theory of particulate processes: analysis and techniques of continuous crystallization. In: *Information Storage and Retrieval (Second)*. Academic Press, Inc., San Diego, CA, USA.

Randolph, A. D. & White, E. T. 1977 Modeling size dispersion in the prediction of crystal-size distribution. *Chemical Engineering Science* **32** (9), 1067–1076. https://doi.org/10.1016/0009-2509(77)80144-9.

Roncal-Herrero, T. & Oelkers, E. H. 2011 Experimental determination of struvite dissolution and precipitation rates as a function of pH. *Applied Geochemistry* **26** (5), 921–928. https://doi.org/10.1016/j.apgeochem.2011.03.002.

Ronteltap, M., Maurer, M. & Gujer, W. 2007 Struvite precipitation thermodynamics in source-separated urine. *Water Research* **41** (5), 977–984.

Ronteltap, M., Maurer, M., Hausherr, R. & Gujer, W. 2010 Struvite precipitation from urine – influencing factors on particle size. *Water Research* **44** (6), 2038–2046.

Saidou, H., Ben Moussa, S. & Ben Amor, M. 2009 Influence of airflow rate and substrate nature on heterogeneous struvite precipitation. *Environmental Technology* **30** (1), 75–83. https://doi.org/10.1080/09593330802505029.

Sakthivel, S. R., Tilley, E. & Udert, K. M. 2012 Wood ash as a magnesium source for phosphorus recovery from source-separated urine. *The Science of the Total Environment* **419**, 68–75.

Samson, E., Lemaire, G., Marchand, J. & Beaudoin, J. J. 1999 Modeling chemical activity effects in strong ionic solutions. *Computing Materials Science* **15**, 285–294.

Schneider, P. A., Wallace, J. W. & Tickle, J. C. 2013 Modelling and dynamic simulation of struvite precipitation from source-separated urine. *Water Science and Technology* **67** (12), 2724–2732.

Shimamura, K., Tanaka, T., Miura, Y. & Ishikawa, H. 2003 Development of a high efficiency phosphorus recovery method using a fluidized-bed crystallized phosphorus removal system. *Water Science & Technology* **48** (1), 163–170.

Siciliano, A. 2016 Assessment of fertilizer potential of the struvite produced from the treatment of methanogenic landfill leachate using low-cost reagents. *Environmental Science and Pollution Research* **23** (6), 5949–5959. https://doi.org/10.1007/s11356-015-5846-z.

Singh, M. R. & Ramkrishna, D. 2014 Dispersions in crystal nucleation and growth rates: implications of fluctuation in supersaturation. *Chemical Engineering Science* **107** (0), 102–113. https://doi.org/10.1016/j.ces.2013.11.047.

Smoluchowski, M. 1917 Mathematical theory of the kinetics of the coagulation of colloidal solutions. *Z. Phys. Chem* **92**, 129–168.

Snoeyink, V. L. & Jenkins, D., 1980 In: *Water Chemistry*, 1st edn., John Wiley & Sons, New York, NY, USA.

Sohnel, O. & Garside, J. 1992 Precipitation: basic principles and industrial applications. In: *Precipitation: Basic Principles and Industrial Applications*. Butterworth Heinemann, Oxford, UK.

Stumm, W. & Morgan, J. J. 1996 *Aquatic Chemistry*. John Wiley & Sons, Inc., New York, NY, USA.

Sun, H., Mohammed, A. N. & Liu, Y. 2020 Phosphorus recovery from source-diverted blackwater through struvite precipitation. *Science of the Total Environment* **743**, 140747. https://doi.org/10.1016/j.scitotenv.2020.140747.

Tai, C. 1999 Crystal growth kinetics of two-step growth process in liquid fluidized-bed crystallizers. *Journal of Crystal Growth* **206** (1–2), 109–118. https://doi.org/10.1016/S0022-0248(99)00300-0.

Talboys, P. J., Heppell, J., Roose, T., Healey, J. R., Jones, D. L. & Withers, P. J. A. 2016 Struvite: a slow-release fertiliser for sustainable phosphorus management? *Plant and Soil* **401** (1–2), 109–123. https://doi.org/10.1007/s11104-015-2747-3.

Tansel, B., Lunn, G. & Monje, O. 2018 Struvite formation and decomposition characteristics for ammonia and phosphorus recovery: a review of magnesium-ammonia-phosphate interactions. *Chemosphere* **194**, 504–514. https://doi.org/10.1016/j.chemosphere.2017.12.004.

Tao, W., Fattah, K. P. & Huchzermeier, M. P. 2016 Struvite recovery from anaerobically digested dairy manure: a review of application potential and hindrances. *Journal of Environmental Management* **169**, 46–57. https://doi.org/10.1016/j.jenvman.2015.12.006.

Tilley, E., Gantenbein, B., Khadka, R., Zurbrügg, C. & Udert, K. M. 2009 International conference on nutrient recovery from wastewater streams. In *Social and Economic Feasibility of Struvite Recovery From Urine at the Community Level in Nepal*. International Conference on Nutrient Recovery from Wastewater Streams, Vancouver, Canada, 10–13 May 2009.

Triger, A., Pic, J.-S. & Cabassud, C. 2012 Determination of struvite crystallization mechanisms in urine using turbidity measurement. *Water Research* **46** (18), 6084–6094.

Türker, M. & Celen, I. 2007 Removal of ammonia as struvite from anaerobic digester effluents and recycling of magnesium and phosphate. *Bioresource Technology* **98** (8), 1529–1534.

Udert, K. M., Larsen, T. a., Biebow, M. & Gujer, W. 2003a Urea hydrolysis and precipitation dynamics in a urine-collecting system. *Water Research* **37** (11), 2571–2582.

Udert, K. M., Larsen, T. a. & Gujer, W. 2003b Estimating the precipitation potential in urine-collecting systems. *Water Research* **37** (11), 2667–2677.

United States EPA 1998 *MINTEQA2/PRODEFA2, A Geochemical Assessment Model for Environmental Systems: User Manual Supplement for Version 4.0*. U.S. Enviromental Protection Agency, Athens, GA, USA.

Van Vuuren, D. P., Bouwman, a. F. & Beusen, a. H. W. 2010 Phosphorus demand for the 1970–2100 period: a scenario analysis of resource depletion. *Global Environmental Change* **20** (3), 428–439. https://doi.org/10.1016/j.gloenvcha.2010.04.004.

Volpin, F., Chekli, L., Phuntsho, S., Cho, J., Ghaffour, N., Vrouwenvelder, J. S. & Kyong Shon, H. 2018 Simultaneous phosphorous and nitrogen recovery from source-separated urine: a novel application for fertiliser drawn forward osmosis. *Chemosphere* **203**, 482–489. https://doi.org/10.1016/j.chemosphere.2018.03.193.

Wang, J., Song, Y., Yuan, P., Peng, J. & Fan, M. 2006 Modeling the crystallization of magnesium ammonium phosphate for phosphorus recovery. *Chemosphere* **65** (7), 1182–1187. https://doi.org/10.1016/j.chemosphere.2006.03.062.

Xu, K., Li, J., Zheng, M., Zhang, C., Xie, T. & Wang, C. 2015 The precipitation of magnesium potassium phosphate hexahydrate for P and K recovery from synthetic urine. *Water Research* **80**, 71–79. https://doi.org/10.1016/j.watres.2015.05.026.

Zekic, A. A., Mitrovic, M. M., Elezovic-Hadzic, S. M. & Malivuk, D. A. 2011 Long-time growth rate changes of sodium chlorate, potassium dihydrogen phosphate, and rochelle salt crystals independent of growth conditions eki. *Industrial & Engineering Chemistry Research* **50**, 8726–8733. https://doi.org/10.1021/ie102425z.

First received 3 October 2022; accepted in revised form 15 February 2023. Available online 2 March 2023